frontiers | Frontiers in Earth Science

TYPE Original Research
PUBLISHED 29 September 2023
DOI 10.3389/feart.2023.1148101



OPEN ACCESS

EDITED BY
Stefan Talu,
Technical University of Cluj-Napoca, Romania

REVIEWED BY
Ana Isabel Ortega-Martínez,
National Research Center on Human Evolution, Spain
Marta Mateu,
Institut Català d'Arqueologia Clàssica, Spain

*CORRESPONDENCE
Nadav Nir,
nadavnnir@gmail.com

RECEIVED 19 January 2023
ACCEPTED 12 September 2023
PUBLISHED 29 September 2023

CITATION
Nir N, Davidovich U, Ullman M, Schütt B and Stahlschmidt MC (2023), The environmental footprint of Holocene societies: a multi-temporal study of trails in the Judean Desert, Israel.
*Front. Earth Sci.* 11:1148101.
doi: 10.3389/feart.2023.1148101



# The environmental footprint of Holocene societies: a multi-temporal study of trails in the Judean Desert, Israel

Nadav Nir[1]*, Uri Davidovich[2], Micka Ullman[2], Brigitta Schütt[1] and Mareike C. Stahlschmidt[3,4]

[1]Department of Physical Geography, Freie Universität Berlin, Berlin, Germany, [2]Institute of Archaeology, Hebrew University of Jerusalem, Jerusalem, Israel, [3]Department of Evolutionary Anthropology, University of Vienna, Vienna, Austria, [4]Human Evolution and Archaeological Sciences (HEAS), University of Vienna, Vienna, Austria

The global distribution of footpaths and their inferred antiquity implies that they are widespread spatial and temporal anthropogenic landscape units. Arid environments are of special interest for investigating historically used footpaths, as older routes may preserve better due to minimal modern impact and slower pedogenic processes. Here we examine footpaths in the Judean Desert of the southern Levant, a human hotspot throughout the Holocene. We studied one modern and two archaeological footpaths (one attributed to the Early Bronze Age and one to the Roman period) using micromorphology, bulk samples laboratory analysis, and remote sensing. Field observations and color analysis indicate that footpaths in the studied arid limestone environment can result in brighter surface color than their non-path surroundings. Similar color changes are reflected using both laboratory analysis and high-resolution remote sensing, where the difference is also significant. Microscopically, the footpaths studied tend to be less porous and with fewer biogenic activities when compared to their non-path controls. However, the two ancient footpaths studied do exhibit minimal indicators of biogenic activities that are not detectable in the modern footpath sample. Our study shows that high-resolution remote sensing coupled with micromorphology, while using appropriate local modern analogies, can help to locate and assess both the environmental effect and the antiquity of footpaths.

KEYWORDS

**micromorphology, albedo, surface, arid, Levant, Roman, Bronze Age, Holocene**

## 1 Introduction

Trails are common human marks on the landscape, occurring in practically all environments (Rodway-Dyer and Ellis, 2018; Loor and Evans, 2021). In the social sciences, it has been argued that both paved and unpaved roads are an important part of our cultural heritage (Jackson, 1984; Zedeño and Stoffle, 2003), while geomorphological research shows that the environmental effects of trails by soil erosion is a problem on a global scale, reaching soil loss rate of 2090 $Mgha^{-1}$ $Y^{-1}$ (Salesa and Cerdà, 2020). Linear soil erosion in particular has recently been suggested to interact with the establishment of new pathways (Sidle et al., 2019). In footpaths, the process of soil compaction through trampling has been studied to some extent in recreational contexts mostly looking at the effect on the local flora (Studlar, 1980; Ayers et al., 2008; Yaşar Korkanç, 2014; Chenhao et al., 2019; Croft, 2019; Sherman et al., 2019). Other types of soil compaction have been investigated through various environments and fields, including the effects of humans, animals,

and vehicles on the subsoil (Liddle, 1975; Eldridge, 1998; Boelhouwers and Scheepers, 2004; Pietola et al., 2005; Botta et al., 2020; Boardman 2022; Tomczyk and Ewertowski, 2023). From a temporal perspective, for a time span of 40 years, using cesium-137 to assess soil erosion due to recreational trail activities, it has been suggested that soil loss is double than that in a control, non-trail area (Rodway-Dyer and Walling, 2010). For longer time spans, gully erosion due to farming as well as the initiation of sunken lanes (i.e., holloways), resulting from erosion and deepening of the pathway, have been dated well into the Holocene (Wilkinson et al., 2010).

As with other types of human-made environmental impacts, it is difficult to assess the timing of the earliest occurrence of footpaths, as an impact that went beyond the environmental imprint produced by other animals (Boelhouwers and Scheepers, 2004; Foley and Lahr, 2015). During the late Pleistocene, human groups traveled long distances to obtain raw materials, and hunter-gatherers likely used similar routes at least on a seasonal basis (Winterhalder, 1981; Malinsky-Buller et al., 2021). However, with the appearance of sedentism, the foundation of settlements and the growth of population would have been accompanied by processes of intensive and repetitive use of trails. Therefore, with the onset of so-called "human niche construction" behavior, an environmental imprint through the repetitive use of trails would become more dominant (Wilkinson et al., 2015). Archaeological evidence for the domestications of both plants and animals marking the emergence of sedentary societies in the Near East dates to ca. 10–8 ka cal. BCE (Gibling, 2018). In our study area, sedentism is also evident in architecture, for example by the monumental walls and tower of Jericho, located in the Dead Sea basin and dated to ca. 8 ka BCE (Bar-Yosef, 1986). Therefore, a minimum age for a unique human imprint on the landscape, by the formation of footpaths, could be situated within the Early Holocene. With respect to the long-term residues of such imprints, i.e., geomorphological and pedological changes related to footpath formation, we present here the study of three footpaths in the Judean Desert.

In landscape-archaeology, the majority of attempts to track down possible prehistoric routes have focused on Least Cost Path (LCP) analysis, or archaeological finds (i.e., pottery, installations, stone tools) discovered along specific routes (Yekutieli, 2006; Schild, 2016; Hardt et al., 2023b), rather than pedogenic or geomorphological evidence. In micro- and geo-archaeology, paved or wheeled-driven tracks have often been investigated using construction materials and micromorphological residues as proxies (Tsokas et al., 2009; Charbonnier and Cammas, 2018). Recently, micromorphology has been used to reveal the application of similar construction methods for centuries of roman road paving (Gutiérrez-Rodríguez et al., 2022). Within archaeological sites, the effect of trampling on pathways and surfaces was thoroughly examined by Rentzel et al. (2017), while others have too used the *in situ* fracturing of microscopic artifacts embedded in sediment as proxies for trampling (Courty et al., 1989; Miller et al., 2010; Nicosia and Stoops, 2017; Goldberg, 2018). Off-site footpaths, however, have been until recently neglected in the geoarchaeological literature (Nir et al., 2022). The long-term effect unpaved footpaths may have on the natural environment is therefore a topic in need for further investigation.

The Judean Desert, a small arid region in the eastern flank of Cisjordan, is an excellent laboratory for the study of ancient pathways due to its limited land use and extreme aridity. The objective of this study, is to uncover comparable patterns and indicators at different scales for the effect footpaths may have on the natural environment, for both modern and long term paths in arid environments. We consider non-wheeled pathways, i.e., footpaths, as trails (>30 cm width) that are reused by humans and at times pack animals in ancient times. Identification of archaeological footpaths is difficult due to post-depositional overprinting, later sedimentary accumulation, and modern land use (Goldberg and Macphail, 2008). In arid environments, however, the influence of these processes is limited, which frequently allows the recognition of archaeological routes, both constructed and unconstructed. The duration of construction and usage of these routes can be time constrained using route-associated material culture, i.e., movement waste and/or road-related structures (Eichhorn et al., 2005). In Nir et al. (2022), the authors have inspected recent and historical footpaths in sub-humid and temperate climatic zones using a variety of methods. Therefore, surface resistance and micromorphological open-source porosity image analysis, that produced effective results in footpaths studied in the latter investigation, were implementable and tested here on footpaths occurring in arid surroundings. Following this notion, in this work, we attempt to further develop tools for documenting and testing the preservation of ancient footpaths in arid environments and their impact on the surface morphology, color and sub-surface of these environments. We couple field description, laboratory analysis on bulk samples and micromorphology of the near surface material to understand the local long- and short-term effects of trampling on the near surface material. Combing these observations from different scales, with local scale pattern analysis of surface structure (stone coverage, color, geomorphology) applying Unmanned Aerial Vehicle (UAV) imagery complemented by soil compaction measurements will allow us to understand the processes trampling has on the near surface material and how it affects the local environment.

# 2 Study area

## 2.1 Geographical and natural setting

The Judean Desert is a 20 km wide (W-E) and approximately 70 km long (N-S) arid region in the rain shadow of the central highland range of Cisjordan. It is geographically framed by the Judean Highlands to the west and the Dead Sea to the east, while the Negev Highlands marks its southern border. The Judean Desert constitutes the western flank of the morphotectonic Dead Sea depression (Garfunkel and Ben-Avraham, 1996). A remarkable attribute of the Judean Desert area is its sharp relief, ranging from ca. 800–1,000 m above sea level (a.s.l.) in the west to approximately 400 m below sea level (b.s.l.) to the east. Locally exposed bedrock units include dolomite, chalk, marl, limestone, and cherts (Lisker et al., 2010). Morphodynamics in the region are characterized by a few yearly flash flood events with exceptionally high sedimentary yield and deposition of slack water deposits and flood sediments. The seasonal flooding results in the abundance of typical arid environment vegetation such as Zygophyllum

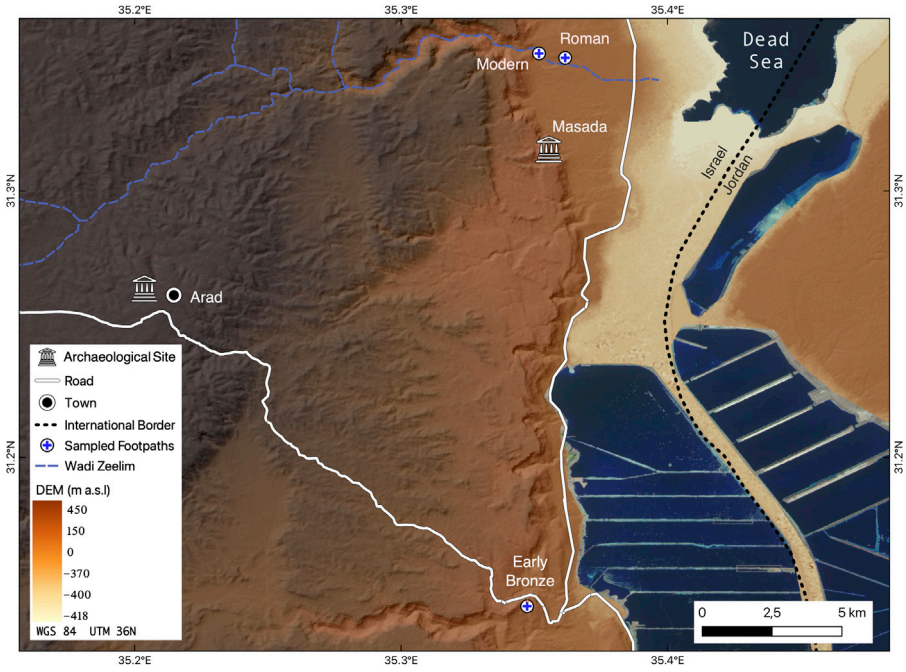


FIGURE 1
An overview map of the study area. Footpaths attributed to the modern and Roman period are located within the Dead Sea plain (northern edge of the figure) while the footpath attributed to the Early Bronze Age (EBA) ascends from the lake shore to the desert uplands (southern edge of the figure). Directly west of the modern city of Arad are the archeological remains of a Bronze Age settlement. also The Digital Elevation Model is based on SRTM (1N31E035V3) available at USGS[1]. Satellite imagery of the water bodies is extracted using the visible light bands from the Sentinal-2 satellite (European Space Agency) available at Copernicus[2]. The underlying slope aspect layer was generated using QGIS (QGIS.org, 2021).

dumosum. The average annual rainfall in research area, at the south-eastern region of the Judean Desert, is 60–80 mm. In the sampling locations, where the modern and Roman period footpaths are located, the surface is composed of a regolith soil, while ca. 20 km to the south, at the Early Bronze Age (EBA) footpath sampling location, bare rock predominates with poorly developed lithosol (Steinberger et al., 1999; Singer, 2007).

## 2.2 Archaeological framework

As a desert strip bounded by settled zones on the west (the Judean Highlands) and east (the Transjordanian Plateau stretching east of the Dead Sea), the Judean Desert has been used intermittently throughout the Holocene as a bridge connecting both sides of the Dead Sea Rift (Davidovich, 2014). Moreover, local Dead Sea Valley products (e.g., salt, bitumen) and commercial cash-crops grown in the oases along the lake shores (palm dates, perfumes) served as important commodities in certain epochs in the history of the greater region, enhancing the development of road networks to mobilize goods and labor, in addition to other activity patterns typifying this region, e.g., refuge in cliff caves (Davidovich, 2013). In tandem, the severe topographical obstacles, created as a result of the tectonic faulting along the western margins of the Dead Sea Transform, limited the use of wheeled traffic in this area. Thus, routes ascending from the rift valley to the desert highlands were used for movement on foot, associated with pack animals (namely donkeys and camels). The Early Bronze Age footpath of the Zohar Ascent (EBA footpath) (Yekutieli, 2009) is part of an east-west route connecting two settled provinces–Arad to the west (Amiran and Ilan, 1978) and the Southeastern Dead Sea communities on the east (Rast, 2001). The ascent is located in the southern part of the Judean Desert, in a segment where the western Dead Sea Escarpment is replaced by a bend scarp (The Har Hemar anticline; Figure 1), locally known as the Wadi (also named Nahal) Zohar/Zeron Outlet. The EBA ascent is the southernmost in a series of routes from multiple periods that pass through this outlet. Along some segments of the ancient route a modern hiking trail is marked (but seldom used); however, the modern segments are easily distinguishable from the ancient footpath both by extremely bright color of the modern path as well as modern waste. The EBA route was identified during a high-resolution regional survey headed by Y. Yekutieli (The survey of the "En-Bokek Map",Israel Antiquities Authority and Ben-Gurion University of the Negev). The surveyors have documented scatters of pottery sherds, consequently noting their location follows a quasi-linear distribution pattern. The footpath studied is located directly within some of the best suited passes for crossing the step topography, a mountain pass on the watershed line between Nahal Hemar and Nahal Zohar drainage basins. The pottery collections were all EBA. Thus, Yekutiely has concluded that these finds represent movement waste of an ancient route (Yekutieli, 2005; Yekutieli,

1 https://earthexplorer.usgs.gov.

2 https://www.copernicus.eu/en.

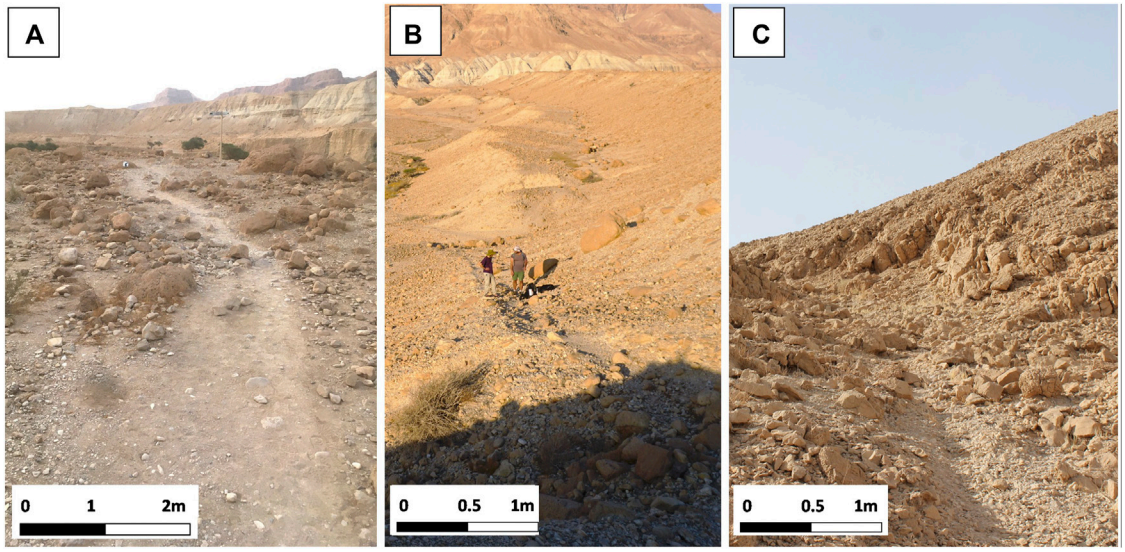


FIGURE 2
Illustrations of the studied Footpaths. **(A)** The modern hiking trail. **(B)** The Roman footpath and **(C)** The Early Bronze Age footpath. Carbonates of the Lake Lisan formation (Pleistocene) characterize the bedrock of the modern as well as of the Roman footpath. Both stretch over alluvial-colluvial sediments at the slope-foot and the ravine fan areas, while the EBA footpath in the Zohar Ascent stretches along a debris-covered backslope.

2006). As the survey proceeded, Yekutieli and his team have located, and later excavated, an EBA-built site on the ridge overlooking the footpath. This was interpreted as a military outpost associated with the use of, and control, over the ascent (Yekutieli, 2009). In later periods, this route was abandoned and more northerly paths were chosen for use (e.g., Aharoni and Rothenebrg, 1960). In the current study, we have selected a segment of the ascent located several tens of meters downslope from a local watershed line where a narrow saddle consists a necessary crossing point (Figures 2C, 3C).

The Roman period in the southern Judean Desert is best known for the construction of the Herodian palace-fortress at Masada, and the historically-documented Roman siege on the Jewish rebels entrenched in the fortress during the Great Revolt between 66 and 73/74CE (Yadin, 1966). The Roman-era road system around Masada has been briefly described by several scholars over the years (e.g., Schulten et al., 1933), and was recently documented as part of a regional archeological survey (Davidovich, 2014). In this study, we examined a segment of the route connecting Masada with the large oasis of Ein Gedi located approximately 20 km to the north; the road was most probably established in association with the efforts of the Roman siege on Masada, and has not been used since, other than by occasional travelers. The road stretches over some kilometers, and we have chosen to examine it in a segment where it is well preserved and list likely to have been distort by post-Roman use. The sampling area was positioned where the path crosses the Pleistocene alluvial deposits (<5°) of Wadi Seiyal (Nahal Zeelim) (Figures 1, 2B), at a segment that it is marked by curbstones along both its sides. Only few meters south of the sampling please as the path is abruptly truncated (>7 m vertically) by the currently active stream (Figure 3A), making it is clear that it has not been used in recent centuries.

# 3 Materials and methods

## 3.1 Selection of footpaths

Selection the two ancient path segments for this research was based on the following criteria: 1) presence of archaeological evidences for the use of the paths, such as structures, stones arrangements and scatters of pottery sherds along the path; 2) The paths were located in a markable distance from currently used trails; and 3) path construction and use can be associated with a distinct period, preferably without evidence of restructuring or extensive usage during later periods. In contrast to that, the modern footpath served as a recent reference and is located on an extensively used recreational route (Wikiloc, 2022). This latter modern footpath was selected based on its relative geographical proximity and environmental similarities to the Roman footpath (Figures 1, 2). Selected trails were sampled in areas where the passing of vehicles could be excluded (or in the case of the Roman segment on the plain area - where it is highly unlikely).

## 3.2 Field observations, mapping and sampling

Sampling included the extraction of undisturbed block samples for micromorphological analysis and bulk samples for bulk laboratory analysis. Following field observation, (Table 2), each footpath was measured along approximately 20 m for its width and slope inclination. Degree of inclination was also measured for the slopes on both sides of the trail. Measurements were taken by t Leica DISTO device. Surface resistance kg/cm$^2$ was measured using a manual penetrometer (ELE pocket penetrometer), with three replicas for each sampling locations (Tejedo et al., 2016). For

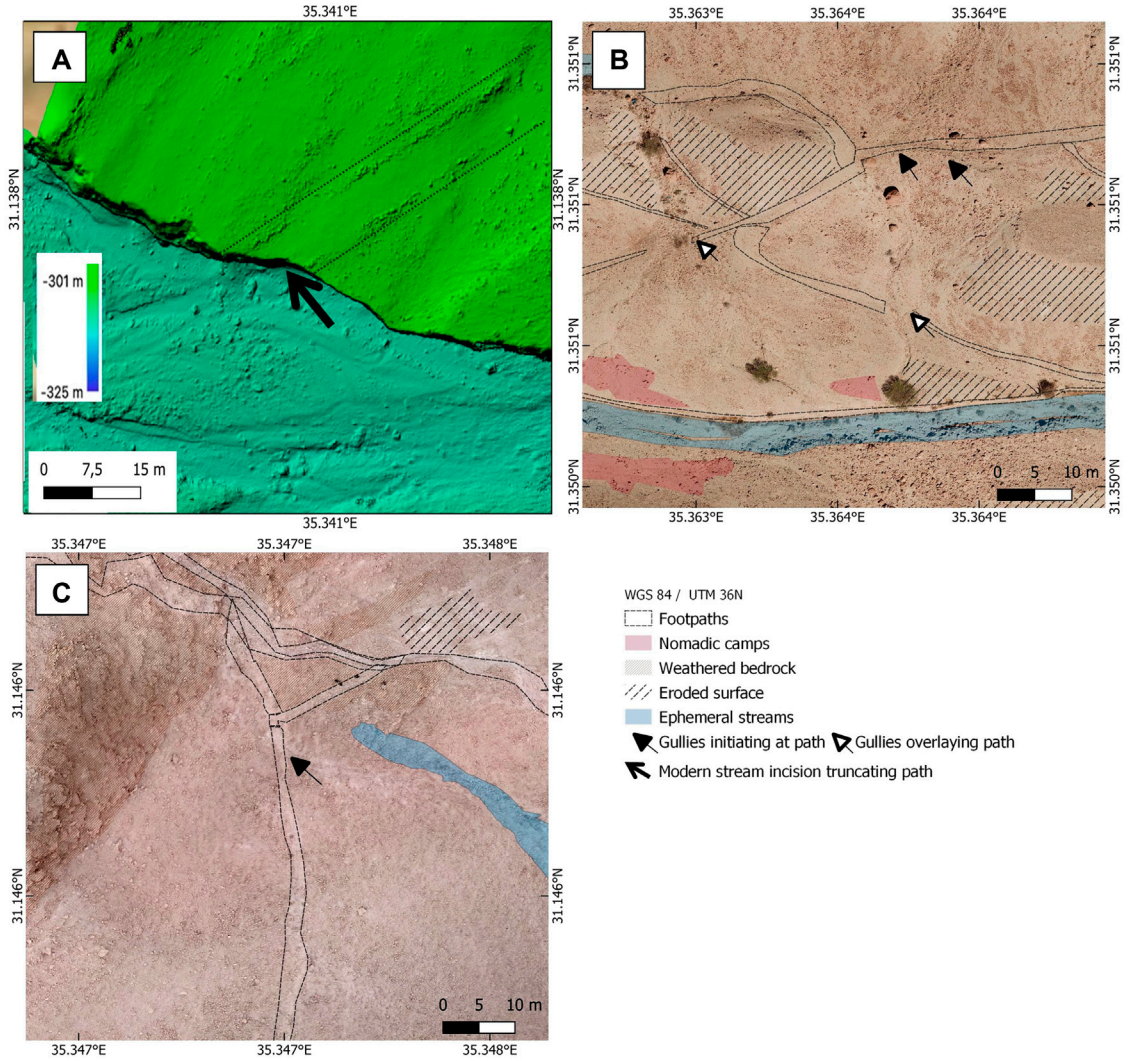


FIGURE 3
UAV image of selected geomorphological features on the archaeologically attributed footpaths; **(A)** DEM of the Roman path on the plane. Notice the approximately 7-m deep truncation by the active stream marked by the black arrow and the curbstones arranged to the sides of the path. **(B)** Orthophoto image of the Roman path segment on the hillslope. Notice the gully fan covering the path's course. **(C)** Orthophoto image of the Early Bronze Age footpath. Notice the gully initiating directly below the path, marked by the black arrow.

each such measurement of the footpath, a control measurement was taken, approximately 1–2 m outside the path's course. Micromorphological samples from the footpaths were also taken, always starting directly at the undisturbed current surface (0 cm) and reaching 5–10 cm depth, depending on the state of the material as it affects sampling depth (i.e., when large pebbles prevented deeper extraction; number of samples=5). Also, outside each footpath, a nearby, undisturbed control was collected (approximately 1–4 m away from the sample within the path), where disturbances due to trampling were not evident ($n$ = 5). Block samples were extracted using plaster of Paris. Bulk samples for laboratory analysis were taken at each micromorphological sampling point and at two additional locations along the paths and at the respective additional off-footpath control samples (Table 1). These bulk samples were each extracted from 0–5 and 5–10 cm below the surface ($n$ = 38). Additionally, bulk samples from 10–15 cm below the surface were taken where unconsolidated fine material occurred in sufficient thickness forming the subsurface material at some footpaths ($n$ = 12).

## 3.3 Remote sensing

Remote sensing imagery data was collected by a UAV using a DJI Phantom 4, RTK. Visible spectrum images above the areas of the two ancient footpaths provided a resolution of approximately 1 cm (Tomczyk et al., 2023). These were geocoded using Agisoft Metashape Pro software and then used for mapping the course of the footpaths. Three archaeologically affiliated footpath segments

**TABLE 1 Footpaths (F) and control (C) sites sampled in the Judean Desert, the location of their coordinates (UTM zone WGS84), and sampling method/parameters.**

| Site | Footpath name | Sample name | Easting | Northing | Bulk sample depths | Micromorphological sample depth and location |
|---|---|---|---|---|---|---|
| Zeelim Wadi Modern recreational trail (surrounding slope angle <10) | Modern footpath | Modern footpath (on a plane) Modern F | 35.35175931° | 31.35166544° | 0–5 cm, 5–10 cm, 10–15 cm | 0–10 cm from the centre of the footpath |
| | | Modern control (on a plane) Modern C | 35.35176387° | 31.35165660° | 0–5 cm, 5–10 cm, 10–15 cm | 0–10 cm deep - 4 m off the footpath |
| Zeelim Wadi Modern recreational trail on hillslope- (surrounding slope angle >20°) | | Modern footpath (on a hillslope) | 35.3520385° | 31.3520789° | 0–5 cm, 5–10 cm | None–as path structure was likely altered for accessibility |
| | | Modern control (on a hillslope) | 35.35213670° | 31.35215208° | 0–5 cm, 5–10 cm | None–as path structure was likely altered for accessibility |
| Zeelim Wadi Roman footpath on plane–(surrounding slope angle <10°) | Roman footpath | Roman footpath (on a plane) Roman F (1) | 35.35889727° | 31.34908704° | 0–5 cm, 5–10 cm | 0–10 cm from the center of the footpath |
| | | Roman control (on a plane) Roman C (1) | 35.35882316° | 31.34918540° | 0–5 cm, 5–10 cm | 0–10 cm, 1 m off the footpath |
| Zeelim Wadi Roman attributed footpath on hillslope (surrounding slope angle >20°) | | Roman footpath (on a hillslope) Roman F (2) | 35.36418741° | 31.35092990° | 0–5 cm, 5–10 cm, 10–15 cm | 0–10 cm from the center of the footpath |
| | | Roman control (on a hillslope) Roman C (2) | 35.36415034° | 31.35094688° | 0–5 cm, 5–10 cm, 10–15 cm | 0–10 cm, 1 m off the footpath |
| Maale Zohar Early Bronze attributed footpath –under saddle | Early Bronze Age footpath | Early Bronze footpath 1 EBA F (1) | 35.34729954° | 31.14631249° | 0–5 cm, 5–10 cm, 10–15 cm | 0–10 cm from the center of the footpath |
| | | Early Bronze control 1 EBA C (1) | 35.34732569° | 31.14629184° | 0–5 cm, 5–10 cm, 10–15 cm | 0–10 cm, 1 m off the footpath |
| Maale Zohar Early Bronze attributed footpath at hill slope | | Early Bronze footpath 2 EBA F (2) | 35.34720145° | 31.14619651° | 0–5 cm, 5–10 cm, 10–15 cm | 0–10 cm from the centre of the footpath |
| | | Early Bronze control 2 EBA C (2) | 35.34717363° | 31.14617519° | 0–5 cm, 5–10 cm, 10–15 cm | 0–10 cm, 1 m off the footpath |

were documented by the UAV; the Roman path on the slope, the Roman path on the plain, and the Early Bronze Age path.

A second step taken was a manual geomorphological mapping of these three segments. For the third step, footpaths and non-path RGB values per pixel were extracted using shape file lines ($n$ = 3 for each path, QGIS) along footpaths and non-path areas, the latter taken at ca. 0.5 m on both sides of the paths ($n$ = 6 for each non-path area). Following the color values extraction, their color values were summed for each GIS shapefile drawn extraction line (approximately 7,000–10,000 pixels) and then averaged. Albedo value were estimated following standard UAV calculation (Wang et al., 2016). However, unlike other UAV studies, the normalization by Landsat 8 values was excluded and replaced by RGB normalization. The latter is sufficient for comparative purposes between path and non-path areas, while additionally the resolution of a 0.5 m wide path would not be detectable by Landsat data (Cao et al., 2018). Therefore, albedo values were calculated using the formula Eq. 1 (Wang et al., 2016):

$$\alpha vis = \frac{0.5621R + 0.1479G + 0.2512B - 0.0015}{256}$$

Remote sensing data were processed in an R environment using the "raster" package for image processing and the "base" package for significance tests ($t$-test at a significance level $\alpha = 0.05$), graphs and box plot visualization (R Core Team, 2013).

## 3.4 Micromorphology

Block samples for micromorphological analysis ($n$ = 10) were impregnated, cut and ground to 30 μm thick thin sections (7 × 5 cm) at the MKfactory in Stahnsdorf, Germany. Thin sections slides were made from the very top part of the samples, so that they would include the recent surface. Analysis of the slides was performed using four magnification ranges (x25, x100, x200, and x400) in plane and cross polarized light (PPL and XPL) and oblique incident light (OIL), on a Zeiss polarizing microscope following standard

micromorphological analysis and terminology (Stoops, 2010; Stoops, 2021; Verrecchia and Trombino, 2021). To characterize porosity, we used optical digitalized void analysis (Pires et al., 2009; Rasa et al., 2012). Images were taken at 1 cm intervals starting at 0.1 cm below the surface and reaching 5 cm below the surface ($n$ = 6 depths). At each depth, using x25 magnification, a triplicate picture was taken on three predetermined and identical locations on the slides ($n$ = 18 per MM slide). Images were then processed using "imager" package in an R environment (R Core Team, 2013) where void cover was automatically assessed. The resulting data indicate the relative porosity of each image (Nir et al., 2022).

## 3.5 Laboratory analysis

Following the results of Nir et al. (2022), complementary laboratory analysis were conducted. Bulk samples were dried at 105°C in a drying cabinet and aggregates were disintegrated using a porcelain mortar. Samples were sieved into coarse (Ø >2 mm) and fine (Ø ≤ 2 mm) material. The Ø ≤ 2 mm fraction was further measured using a LS 13320 PIDS Beckmann Coulter Laser particle size analyzer to obtain the grain size distributions. The Ø ≤ 2 mm fraction was additionally used for further geochemical and mineralogical analyses ($n$ = 60). The respective sample preparation and measurement steps were conducted according to previously published workflows (Nykamp et al., 2020; Hardt et al., 2023a). Measurement of the electrical conductivity (μS $cm^{-1}$) and pH values of the water-saturated samples ($n$ = 50) was determined in a 1:2.5 solution of 10 g of air-dried sediment and 25 ml of bi-distilled water, using handheld electrical conductivity and pH (with a resolution of 0.1) meters accordingly (Hanna Instruments). Total carbon (TC) content was determined using a LECO Truspec CHN and an add-on elemental analyzer ($n$ = 50). Total Organic Carbon (TOC) was measured following CaCO3 dissolution using catalytic oxidation at 680°C and subsequent Non-Dispersive Infra-Red detection using a TOC-L Shimadzu device ($n$ = 50). Mineralogical X-Ray Diffraction (XRD) values were determined by inserting flat-surfaced samples on metal pellets into a Rigaku Mini-flex 600 X-Ray Diffractometer ($n$ = 15). Elemental analysis was carried out using the p-ED-XRF (portable energy-dispersive X-ray fluorescence) analyzer Thermo scientific Niton XLt3. Each XRF sample was placed in plastic cups and sealed with a mylar foil (0.4 μm). The prepared sample-cups were placed on the p-ED-XRF and measured for 120 s with different filters for detecting specific elements ($n$ = 60). Measurements included four known reference standards (RF3, RF25, RF87, RF89) measured prior to and following the sample measurements for device error assessment and calibration. Further elemental analysis was conducted using Inductively Coupled Plasma-Optical Emission Spectrometry (ICP-OES) following digestion in aqua regia (HNO3 + 3 HCl). ICP-OES measurements were conducted in the Julius Kuhn Institute (JKI) Berlin ($n$ = 50). Measurements included three reference materials and a black sample. Color band values were obtained using a Minolta Portable Spectrophotometer CM-2600d using the CIELAB color space (D65 European midday standards). A triplicate was measured for each sample under three different runs of the instrument which included white and room light measurements for calibration. The data was further normalized by dividing each color band by the total RGB sum and being placed on a logarithmic ratio in the R environment (R Core Team, 2013).

# 4 Results

## 4.1 Field observations

### 4.1.1 Modern footpath (zeelim wadi)

The part of the modern footpath examined includes a segment where the footpath is descending on a south-facing slope of ca. >15° ("hillslope"), from a plateau-like area (in Pleistocene floodplain and colluvial deposits), towards a lower plane area of approximately <5° inclination ("plane"), one that is truncated by the current Zeelim channel (Table 1). The examined segment of the path on the hillslope is approximately 80 m long, while on the plane area, the examined footpath segment is approximately 150 m long. The non-path areas were generally occupied by large (approximately 10–90 cm Ø), dark brown (dust and bacterial cover), and angular boulders. These boulders were sparsely dispersed and in the areas between them, homogeneous fine material was present ("soil crust"; Cole, 1990). The approximately 0.5–1-m wide (Table 3) footpath surface is covered with subrounded limestone and chert boulders and large pebbles (approximately 5–30 cm Ø) within and overlaying compacted fine sands and silt (Table 2). At some locations along the plane, the path is approximately 2–4 cm deeper than its surroundings (i.e., sunken). One minor gully (10–50 cm deep and 1 m wide) evolves directly below the path at the hillslope (>15°) segment (Figure 2A).

### 4.1.2 Roman footpath (zeelim wadi)

The Roman footpath is similarly composed of two segments, running on a hillslope (>15°) and on a plane (<5°) area, approximately 1 km southeast of the modern footpath sampling point (Table 2). On the hillslope, the footpath runs for roughly 200 m (approximately 1 m wide) semi-diagonally along a south-facing slope in NE-SW direction and descends south-westwards to a Lower Pleistocene terrace plane area. On the plane, the footpath runs for 450 m; here the footpath is generally 5 m wide and at parts, it is marked by a line of >20 cm curbstones on both sides (Figures 2B, 3). The path occasionally crosses gullies, 1–2 m deep, functioning as first to second-order ephemeral streams. As it continues southwest, at one of its better-preserved areas, the path is abruptly truncated by a > 7-m deep incision of the active stream cutting into its own deposits (Figure 3A). The areas adjacent to the path are covered by boulders (approximately 6–40 cm Ø) and shrubs with fine material occupying the surface between them ("desert crust"), while boulders lying on the paths generally show sizes of 3–20 cm Ø and are not accompanied by vegetation.

### 4.1.3 Early bronze age footpath (zohar ascent)

The Early Bronze age (EBA) footpath stretches on mostly bare bedrock from the northwest and crosses a watershed line through a saddle. In the current study, the footpath was examined where it crosses the saddle and continues to run on the east-facing hillslope (Table 1). The footpath is approximately 1 m wide and 75 m long in the sampling area. Under the saddle, it is composed of 3 broken segments of approximately 10-m long paths. These path segments descend semi-perpendicular to the slope on bare rock and patches of sediments. Some of these segments had coarse and fine grains cemented together in a 'breccia-like' surface. From the area below the saddle, on the southeast-facing hillslope, an officially marked modern trail, which does not show intensive usage, continues to the

**TABLE 2 Field observations and measurements.**

| Site | Surface morphology | Surface texture | Compaction [kg/cm$^2$] | Path/non-path slope [°] | Path width [m] | Profile description (20 cm depth) |
|---|---|---|---|---|---|---|
| Modern footpath control sample (1) | River terrace/floodplain confined by the recently active Zeelim stream and a higher terrace. One gully and the is truncating the plane surface | Concentrations of the larger subrounded pebbles composed of various limestones and cherts (>20 cm) in bands. Underlining the pebbles and between them are accumulation of the silts, fine sands and gravels | 3.8 ± 1.2 | −14°, −6°, −4°, −5°, −10° | | Silts and fine sands and gravels constitute the upper ca. 2–3 cm. Gravel grain size increase at 2–3 cm along with subrounded pebbles. Loose brown sediments with no compaction |
| Modern footpath, footpath sample (1) | The footpath segment runs semi parallel to the recently active Zeelim stream | Even distributions of subrounded to subangular pebbles in different sizes (<1 cm - >5 cm) pebbles composed of various limestones and cherts imbedded in silt-gravel matrix | 4.7 ± 0.6 | −1.2°, -2°, −3.5°, −6.1°, −2.2° | 0.75, 0.72, 0.55 | Subrounded pebbles (>2 cm in diameter) and coarse gravels in silty matrix, homogenic for the entire 20 cm. Minimally compacted light brown sediments with loos silty pockets |
| Roman footpath plane (1) control sample | River terrace/floodplain confined by the recently active Zeelim stream and a higher terrace. Several gullies and 5–20 cm wide paths are crossing the plane surface | Fan sediments in concentrations of the larger subrounded pebbles composed of various limestones and cherts (>20 cm) in bands. Underlining the pebbles and between them are accumulation of the silts, fine sands and gravels | 4.4 ± 0.9 | south of path 0°, −3.9°, −2.6° north of path 0.7°,– 0.6°, −0.2° | | Subangular to rounded (1–10 cm in diameter) pebbles and gravels for the entire 20 cm. Lamina of 1–3 cm thick red-brown silt parallel to the surface angle starting at 0.5 cm below surface. Below the lamina, loose light brown silty matrix between pebbles and gravels with no compaction |
| Roman footpath plane (1) footpath sample | The 5 m wide footpath segment crosses the Zeelim Wadi fan diagonally | It is marked by natural pebbles >20 cm situated to its sides. The path is truncated (ca. 7 m south of sampling point by more recent Zeelim stream to form a >10 m profile. Fan sediments on the path are mostly cemented. 1–5 cm sub angular to rounded pebbles composed of various limestones and cherts are common | 4.8. ± 0.3 | 2.35° | 5.60, 5.15, 5.5 | Subrounded pebbles (1–3 cm in diameter) and coarse gravels in silty matrix constitute the upper ca. 3 cm. Below that, the silt component increases and is more dominant. Compacted light brown sediments at the upper 3 cm with very few silty loose light brown pockets below 3 cm |
| Roman footpath hillslope (2) control sample | The area of the hillslope between the plane and the upper river terrace with common rills and gullies running parallel to the slope angle and few footpaths diagonal to it | Subrounded to angular pebbles at different sizes (<2 cm) and (>10 cm) composed of various limestones and cherts organized in bands. Underlining the pebbles and between them are pockets of silts and fine sands | 4 ±1.5 | Above path: 24.4°, 24.9°, 27.05° Below path: −30.1°, −23.5°, - °28.2 | | Located in a silty pocket between 20 cm boulders that are banded on the surface. Subrounded to subangular pebbles (5–15 cm in diameter) and coarse gravels dominant throughout the profile in a silty matrix. Minimally compacted loght brown sediments with loose silty pockets |
| Roman footpath hillslope (2) footpath sample | The ca. 1 m wide footpath segment descends diagonal to the slope angel into the plain area | The surface is composed of rounded to subangular pebbles at different sizes (<2 cm) and (>5 cm) pebbles composed of various limestones and cherts. Occasional large (>20 cm) stones are observed to its sides and few of these are also overlying it | 4.8 ± 0.3 | 11.8° | 1.3, 1.6, 1.15 | Subrounded to subangular pebbles (5–10 cm in diameter) and coarse gravels dominant throughout the profile in a silty matrix. Minimaly compacted light brown sediments with loose silty pockets |

(Continued on following page)

**TABLE 2 (*Continued*) Field observations and measurements.**

| Site | Surface morphology | Surface texture | Compaction [kg/cm$^2$] | Path/non-path slope [°] | Path width [m] | Profile description (20 cm depth) |
|---|---|---|---|---|---|---|
| EBA footpath hillslope (1) control sample | The surface of the slope directly beneath the watershed line is composed of exposed limestone bedrock, colluvial subangular gravels and boulder Larger than 30 cm. A main dry channel drains the area and 3 gullies serve as tributaries, with one of them initiating from the footpath surface | The boulders generate natural traps that form pockets of finer sediments (silt-fine sand) | 3.2 ± 1.4 | Above path: 19.1°, 26.3°, 24.75° Below path: −17.3°, −15.8°, −31.2° | | Located upslope from the footpath in a silty pocket between 20 cm boulders that are banded on the surface. Upper 2 cm are dominated by silt, subangular to angular pebbles (5–7 cm in diameter) appear at 1–2 cm below surface with silt patching between them. Minimally compacted brown sediments with loose silty pockets |
| EBA footpath hillslope (1) footpath sample | The ca. 1 m wide footpath segment descends parallel and diagonal to the slope angel directly under the saddle | The surface is of the path is cemented and composed of angular to subangular gravels and boulders composed of various limestones and cherts, imbedded in silty-sand matrix | 5 ± 0 | 10.6° | 1.25, 0.8, 1.25 | Angular to subangular pebbles in silty matrix. Homogenous structure appears throughout the 20 cm. Compacted light brown sediments at the upper 3 cm and looser below |
| EBA footpath hillslope (2) control sample | The boulders generate natural traps that form pockets of finer sediments (silt-fine sand) | The surface of the slope is composed of exposed limestone bedrock, colluvial subangular gravels and angular boulder Larger than 30 cm | 4.3 ± 0.8 | Above path: 21°, 20°, 27° Below path: 35° (the gully), 34°, 17° | | Located in a silty pocket between boulders downslope from the footpath. The upper 1 cm is dominated by silt, subangular to angular pebbles (5–7 cm in diameter) appear throughout the profile on a silt matrix. Minimally compacted brown sediments with loose silty pockets |
| EBA footpath hillslope (2) footpath sample | The ca. 1 m wide footpath segment descends perpendicular to the slope angel. A gully initiate at this footpath's surface. Downslope on the footpath, after the gully stars, water seem to flow on the path itself and some incision occur (>10 cm, <20 cm deep, i.e. sunken lane) | The surface is of the path is composed of angular to subangular gravels and boulders composed of various limestones and cherts, imbedded in silty-sand matrix | 4.6 ± 0.9 | 9°, 16°, 11° | 0.76, 1.32, 0.85 | The upper 3 cm is dominated by silt, below, subangular to angular pebbles (5–7 cm in diameter) appear throughout the profile on a silt matrix. The upper 1 cm is light brown and compacted, at 2–3 cm below surface it is dark brown and below that depth sediments are light brown loose silty pockets between the pebbles |

northeast. A second segment of the path continues to the southwest on the hillslope. On the latter segment, as the path runs perpendicular to the slope, a gully evolves directly from the surface of the footpath. The footpath surface is covered with subangular pebbles (approximately 5–60 cm Ø) within sands and silt (Table 2). Poorly sorted debris of angular rock fragments reaching up to boulder sizes cover most of the non-path surface while silt-fine sands occupy the areas between the boulders (Figures 2C, 3C).

For all footpaths, surface penetration resistance is significantly higher than non-footpath surfaces (*t*-test $p < 0.05$, $n = 28$). In the Zeelim Wadi, control samples have a compaction of 3.8 ± 1.2 (for the modern path area) and 4.4 ± 0.9 (for the Roman path area) while footpaths show higher values of 4.7 ± 0.6 (for the modern path) and 4.8. ± 0.3 (for the Roman path). The same trend is apparent in the measurements of the Zohar Ascent (Early Bronze Age); controls show values between 3.2 ± 1.4 and 4.3 ± 0.8, while the footpaths have values of 5 ± 0 and 4.6 ± 0.9 (Table 2).

## 4.2 Local scale pattern analysis

All sampled footpaths were observed to be brighter than their surroundings while their compacted surfaces seem to encourage overland flow, affecting local morphodynamics. Following the latter observations, we expected to find differences in the color measurements on and around the surface of trails compared with non-path areas.

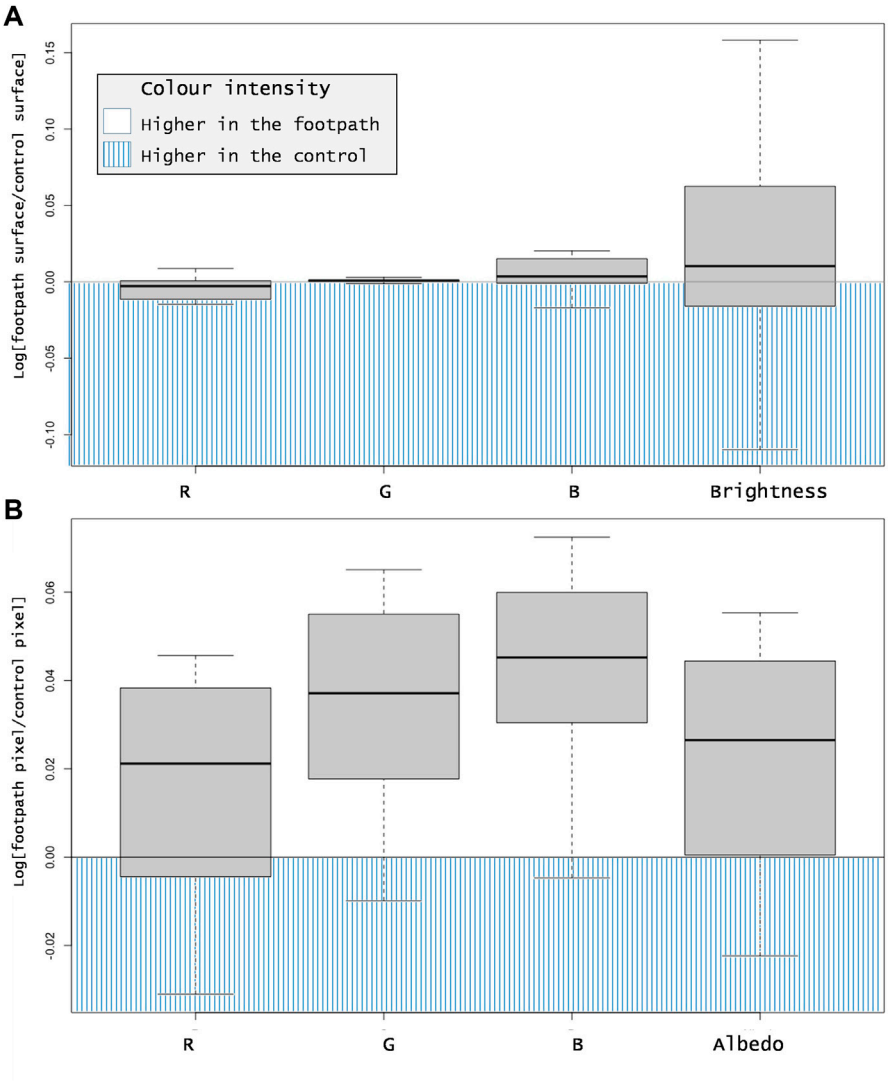


FIGURE 4
Color evaluations of two archaeological footpaths. The footpaths color values are plotted against their corresponding non-path areas in logarithmic scale. The median average is marked by a black horizontal line within the boxplot. **(A)** RGB (Red, Green, Blue) and brightness values of the fine fraction (<2 mm) originating from footpaths ($n$ = 30) vs. their respective control samples ($n$ = 30). **(B)** RGB and calculated albedo orthophoto values originating from footpaths vs. their respective control samples (each n >10000 pixels). Notice both brightness ($p > 0.05$) and albedo ($p < 0.05$) values are higher on the footpath surfaces than on the non-path areas.

Color measurements of the fine fraction (<2 mm) show consistent differences between footpaths and their control samples (Figure 10). It is evident that footpaths have brighter color values and higher values for the green and blue bands than their controls (Figure 4A). Differences in the blue spectrum values between samples extracted from footpaths and their control samples are significant ($p < 0.05$) while the green values are insignificantly different between footpath and non-footpath areas ($p > 0.05$). Additionally, three sections were mapped using a UAV orthophoto image to extract the RGB signature of the footpaths and their neighboring areas; Roman footpath (1) situated on the plane topography, Roman footpath (2), its continuation on the hillslope, and the Early Bronze footpath segment. The extracted RGB values from triplicate lines marked on the footpaths show higher RGB values than the same lines placed approximately 1 m on both sides of the paths (Figure 4B). Based on the RGB values, albedo values were calculated to assess the possible reflection effect of the footpaths. There are higher albedo values on the surfaces of the footpaths compared to the non-path control areas (Figure 4). This difference is relatively small with a median of +2.7% and with the highest difference value lying at +5.7% for the EBA footpath, however, it is significant ($p < 0.05$).

## 4.3 Laboratory analysis

To examine whether the patterns described in the previous section (4.2) are affected structural subsurface processes or triggered by surface processes and, we compare the average characters of the surface material extracted from 0–5 cm depth (color, grain size, bulk parameters, selected elements) with the corresponding data of all samples (0–5, 5–10, 10–15 cm).

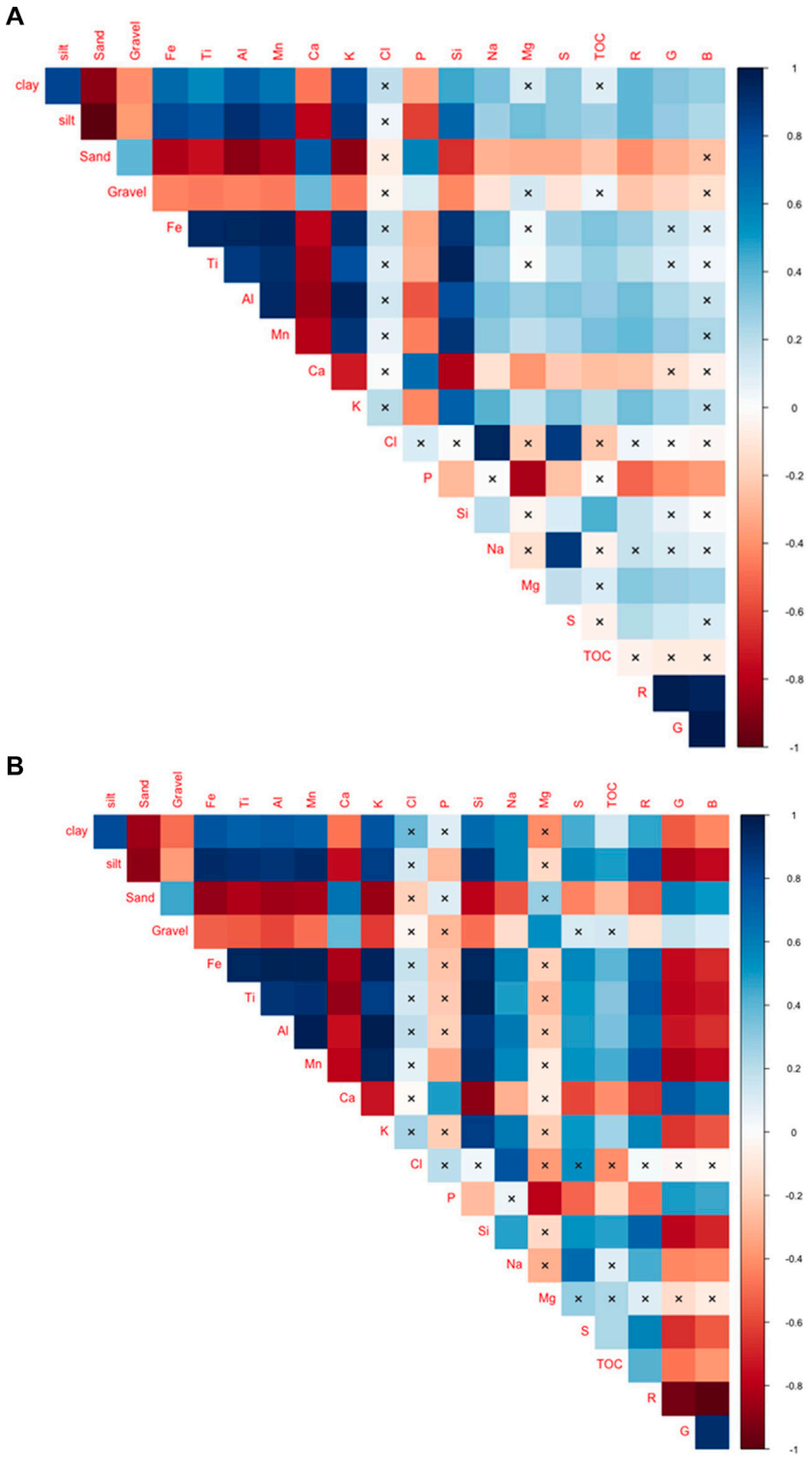


FIGURE 5
Correlation analysis (R "corrplot" package) between various data types; **(A)** all samples and **(B)** surface samples ($n$ = 50 and $n$ = 20 accordingly). X marks an insignificant correlation ($p > 0.01$). Positive correlations are colored coded in blue (max = 1) while negative ones are in red (max = −1). Grain sizes were assessed using a Coulter Laser particle size analyzer while elemental data was obtained using ICP-OES following digestion in aqua regia (HNO3 + 3 HCl), apart from chlorine which was measured in p-ED-XRF. Gravels were calculated by weight based on sieving. TOC was directly measured using Non-Dispersive Infra-Red detection. Color band values were obtained using a Minolta Portable Spectrophotometer.

**TABLE 3 Micromorphological description of the footpaths and control samples.**

| Sample | Context | Microstructure and features | Components[a] | Interpretation | SI figures |
|---|---|---|---|---|---|
| Modern footpath control sample (1) | River terrace/floodplain | Enaulic to closed porphyric, massive, poorly sorted. No to -Subhorizonal orientation of the coarse material. Complex packing voids, vesicles, subhorizonal planes, vughs, dusty clay coating, iron/manganese oxide nodules (20–120 μm Ø) with regular outline. Calcarous-cementation (plant roots). Alternating grain supported and fine clay dominated layers with vesicles (slaking crusts) | Light grey brown clay, calcitic crystallitic b-fabric. Micritic limestone rock fragments: medium sands to fine gravels. Chert: Subangular to subrounded coarse sands to fine gravels. Quartz: subrounded to subangular fine sands. Few subangular shell fragments | Shortly transported aggregates (100–1,000 μm Ø). Interchanging medium and low energy depositions, seasonal plant active (roots) following water saturation | 4a-c |
| Modern footpath, footpath sample (1) | Intensely used ca. 0.7 m wide footpath segment on a plane area | Closed porphyric to enaulic, massive, poorly sorted. No to subhorizonal orientation of the coarse material. Complex packing voids, vughs, iron/manganese oxide nodules (20–100 μm Ø). At 4 cm below surface, enaulic to coarse monic | Light grey brown clay, calcitic crystallitic b-fabric. Micritic limestone rock fragments: Subangular to subrounded medium-coarse Sands. Chert: Subangular fine gravels. Quartz: subrounded to subangular silts to fine sands | Compacted upper 4 cm overlaying medium energy deposition | 5a-b |
| Roman footpath plane (1) control sample | River terrace/floodplain | Enaulic to coarse monic, massive, poorly sorted. No orientation of the coarse material. Complex to simple packing voids. At 3 cm below the surface, an approximately 1 cm thick, horizontal clayey microlayer is evident. Below this microlayer are alternating grain supported and matrix dominated layers | Light grey brown clay: as matrix and in subangular aggregates, micritic limestone rock fragments: Subrounded fine gravels | Pedogenic activities and medium energy deposition | 6a-b |
| Roman footpath plane (1) footpath sample | Rarely used 5 m wide footpath segment bounded by pebbles | Closed porphyric to enaulic, massive, apedal to granular, poorly sorted. No orientation of the coarse material. Vughs, planes and complex packing voids | Light grey brown silt-clay, calcitic crystallitic b-fabric. Micritic limestone rock fragments: Subrounded medium-fine sands to fine gravels. Quartz: subrounded silts to fine sands. Mica: subangular fine sands | Calcareous cementation through redeposited calcite via seasonal plants roots and the following bacterial activities and mechanical compaction from the surface | 7a-b |
| Roman footpath hillslope (2) control sample | The area of the hillslope between the plane and the upper river terrace | Enaulic to closed porphyric, massive, unsorted. No orientation of the coarse material. Complex packing voids, Iron/manganese oxide nodules (20–100 μm Ø). At 2.5 cm below surface, Subhorizontal orientation of the coarse material, slacking crusts with subhorizontal planes, channels and vughs | Light brown clay. Micritic limestone rock fragments: Subangular to angular medium-coarse sands. Subangular to subrounded fine gravels to pebbles. Quartz: subrounded fine sands | Non *in situ* but rather transported - aggregates (100–2000 μm Ø). Colluvium and low energy depositions and bioturbation | 8a-b |
| Roman footpath hillslope (2) footpath sample | The ca. 1 m wide footpath segment descends diagonal to the slope angel into the plain area | Enaulic to porphyric, massive, unsorted. No orientation of the coarse material. Complex packing voids | Light brown silt-clay, calcitic crystallitic b-fabric. Micritic limestone rock fragments: Subangular to rounded fine gravels to pebbles. carbonate grains: Subrounded fine-medium sands. Chert: Subangular to subrounded fine gravels. Quartz: subangular to subrounded silts to medium sands | Colluvium and medium energy depositions | 9a-b |
| EBA footpath hillslope (1) control sample | Hillslope directly beneath the watershed line composed of exposed limestone bedrock, colluvial subangular gravels and boulder | Enaulic to closed porphyric, massive and channel, unsorted. No orientation of the coarse material. Complex packing voids, channels. Slacking crusts with planes | Light brown clay, calcitic crystallitic b-fabric. Micritic limestone and chalk rock fragments: Subrounded medium-coarse sands to pebbles. Few quartz: subrounded silt to fine sands | Colluvium, low energy depositions and water saturation | 10a-b |

(Continued on following page)

**TABLE 3 (*Continued*) Micromorphological description of the footpaths and control samples.**

| Sample | Context | Microstructure and features | Components[a] | Interpretation | SI figures |
|---|---|---|---|---|---|
| EBA footpath hillslope (1) footpath sample | A ca. 1 m wide footpath segment descends parallel and diagonal to the slope angel directly under the saddle | Closed porphyric to enaulic, massive, poorly sorted. No orientation of the coarse material. Complex packing voids, vughs. Iron/manganese oxide nodules (20–150 μm Ø) | Light brown silt-clay, calcitic crystallitic b-fabric. Micritic limestone and chalk rock fragments: Subangular to subrounded medium-coarse sands to fine gravels. Shells: Subangular to subangular sands. Few quartz: subrounded silts to fine sands | Low to medium energy deposition and minimal mechanical compaction from the surface | 11a-b |
| EBA footpath hillslope (2) control sample | Hillslope directly beneath the watershed) | Enaulic, massive, unsorted. No orientation of the coarse material. Complex packing voids, vughs, Iron/manganese oxide nodules (20–100 μm Ø) | Light brown clay, calcitic crystallitic b-fabric. Micritic limestone and chalk rock fragments: Subangular to subrounded fine gravels. Shells: Subangular to subangular coarse sands to gravels. Few mica: subangular fine sands | Minimal cementation through redeposited calcite via seasonal plants and following bacterial activities. High and low energy depositions | 12a-b |
| EBA footpath hillslope (2) footpath sample | A ca. 1 m wide footpath segment descends perpendicular to the slope angel | Enaulic to closed porphyric, massive, unsorted. No to -subhorizonal orientation of the coarse material. Complex packing voids, planes, vughs, vesicles, iron/manganese oxide nodules (20–100 μm Ø). Slacking crusts with fissures | Light grey brown silt-clay, calcitic crystallitic b-fabric. Micritic limestone and chalk rock fragments: Subangular to subrounded medium-coarse sands to fine gravels. Few quartz: subangular to subrounded silts to fine sands | Colluvium, low energy depositions, water saturation and compaction | 13a-b |

[a]listed by decreasing abundance.

Calcium and silicon are the dominating elements in all samples (Supplementary Figure S1). Texture of all samples is a sandy loam. Grain size, pH, EC and elemental analysis of the bulk samples did not show consistent differences between the footpaths and their controls and are presented in the Supplementary Material (Supplementary Table S1). Using correlation analysis some correlations emerged: In all samples the finer fraction tends to positively correlate with iron, titanium, aluminum, and manganese (Figure 5). Contrastingly, calcium concentrations are positively correlated with the occurrence of the sand fraction and negatively to the occurrence of the silt fraction. Sodium, chloride, and sulfur concentrations are strongly correlated with each other, although sodium and chlorine occur in low concentrations (Supplementary Figure S1; Blum 1997). Spectral data referring to the RGB color space do not show strong relationships to any of the elements or grain sizes when looking at the total samples ($n$ = 50). Considering exclusively the near surface samples (0–5 cm) some correlation is evident: within all surface samples ($n$ = 20), red band values are positively correlated with silt, manganese and silicon ($\alpha < 0.05$), and negatively correlated with calcium ($\alpha < 0.05$); while green and blue band values show a mirror image, being negatively correlated with silt, manganese and silicon ($\alpha < 0.05$), and positively correlated with calcium ($\alpha < 0.05$) (Figure 5, Supplemantary Table 1).

## 4.4 Micromorphology

Similar mineralogical composition, originating from the exposed weathered bedrock and soil surfaces, is evident in all samples (Figure 5; Supplementary Figure S1). Particularly abundant are carbonate grains and rock fragments (limestone), and silicates (chert, quartz). The following descriptions depict the post-depositional differences related to footpath use between footpath and control samples wherever these are evident. A micromorphological description of all thin sections can be found in Table 3.

For the Modern footpath, the control sample shows iron/manganese oxide nodules with regular outline and calcareous-cementation (plant roots). Alternating grain supported and fine clay dominated layers occur with vesicles (slaking crust). The latter are likely the result of water saturation (e.g., puddle) and trapped air. The footpath samples are absent of calcareous-cementation, we observed no alternating layers or vesicles. At 4 cm below surface, a micro-structural change occurs, the c/f related distribution changes here from coarse monic to enaulic, while the upper 4 cm present medium energy deposition (Table 3; Figure 6).

The footpath attributed to the Roman period was sampled both on a (1) plane and a (2) hillslope (Figure 7) area. For the footpath located on the plane, Roman footpath (1), in the control sample, light grey brown clay is evident as matrix and in subangular aggregates. Additionally, at 3 cm below the surface, an approximately 1 cm thick, horizontal clayey microlayer is evident, below which, alternating matrix and grain supported units occur. The clayey microlayer and alternating matrix and grain supported units are the result of seasonal water saturation and medium energy deposition. In the footpath sample, no subangular aggregates or clayey layer are evident, while we observed some calcareous cementation through redeposited calcite. The subangular aggregates and clay layer in the control sample represent natural

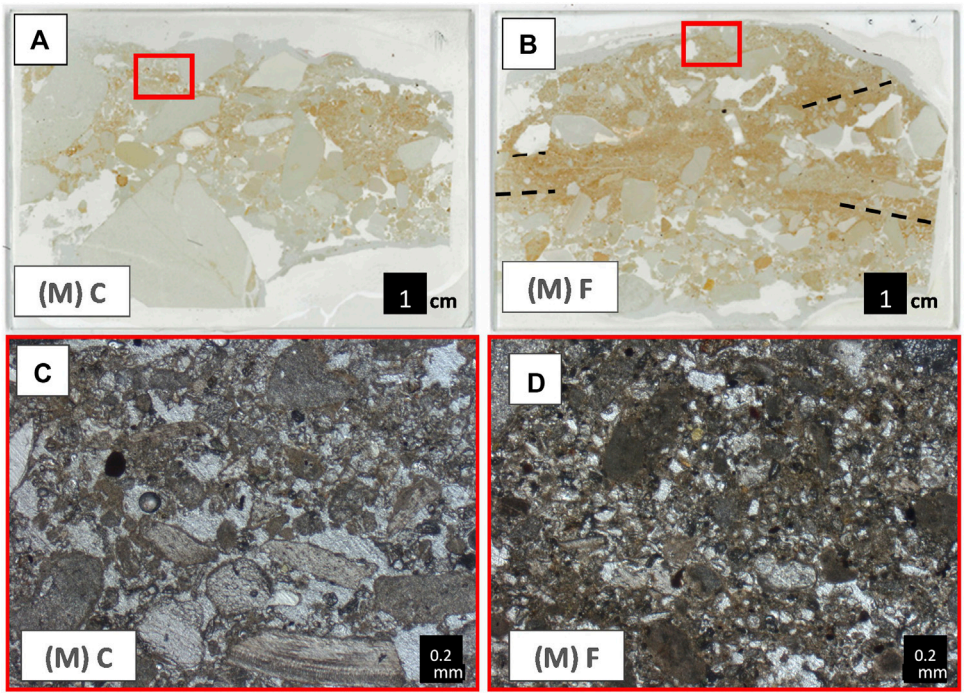


FIGURE 6
Thin section scans and microphotographs (PPL) of the modern (M) footpath (F) and its control (C) sample. Red boxes in the thin section scans indicate the location of microphotographs. **(A)** Scan of non-path control sample, which is dominated by coarse grains. **(B)** Scan of footpath sample showing three distinct units, where silt and clay dominate over coarse grains in the upper subunit, underlain by a bedded subunit (dashed lines) and the bottom subunit is dominated by coarse grains. **(C)** Open enaulic microstructure in the footpath control. **(D)** Closed phorphyric microstructure in the footpath samples from the upper subunit.

accumulation and surface formation processes, while their absence in the footpath sample could be the result of surface compaction, i.e. trampling causing the destruction of aggregates and homogenization of microstratigraphic sequences. Additionally, water percolation is hindered, leaving the subsurface unsaturated and by doing so, decreasing the ability to form aggregates. The calcareous cementation related to plant growth and visible in the footpath sample could indicate periods of surface stabilization.

At the hillslope area, Roman footpath (2), in the control sample, aggregates are evident (100–2000 µm Ø) as well as iron/manganese nodules. At 2.5 cm below surface a subhorizontal orientation of the coarse material as well as slacking crusts with subhorizontal planes, channels and vughs are visible. The above mentioned aggregates do not seem to present an *in situ* formation process but are rather transported as colluvial material. The sample represents low energy depositions and bioturbation. The footpath sample lacks similar transported aggregates, neither did we observe channels here. Therefore, the foothpath samples also represent colluvium deposits, but with no clear indication of bioturbation or post depositional features.

The footpath associated with the Early Bronze Age is located close to the watershed line. The footpath was sampled in two locations on the south-facing slope, both with steep slope angles (>15°). The first Early Bronze footpath segment was sampled directly below the saddle (EBA footpath (1)), while the second was sampled on the hillslope (EBA footpath (2)). For both samples, little distinct patterns that differentiate the footpaths from the control samples were observed (Table 3; Figure 7).

For EBA footpath (1), the control sample has complex packing voids, channels and slacking crusts with planes. The latter observation along with subrounded medium-coarse sands to pebbles (see Table 3) suggest colluvial accumulation and low energy deposition with little indication of post depositional processes. Similarly, the footpath sample shows low to medium energy deposition with additionally some minimal mechanical compaction from the surface resulting in slightly smaller grain size distribution (absent of pebbles) and a c/f related distribution that is more closed porphyric than enaulic.

For EBA footpath (2), the control samples shows similar characteristics to the EBA footpath (1) samples, including complex packing voids, planes, vughs and iron/manganese oxide nodules. However the EBA (2) control sample additionally presents a few areas with calcareous cementation. The latter is the result of redeposited calcite via seasonal plants and following bacterial activities. The EBA (2) footpath sample has similar characters as its control sample but with additional slacking crusts with fissures while calcareous cementation was not evident for the footpath sample.

Triplicated porosity measurements at a microscopic level showed that the subsurface of the footpaths at the 5 sampling points tends to be less porous than their respective control samples (Figure 10B). This is especially true for the surface (i.e. the uppermost 0.1 cm) where all footpaths are less porous ($p<0.05$) than their control samples (Figure 10C). The modern footpath sample shows the lowest porosity of all case studies compared with its control sample, especially for the upper 3 cm below the surface. Deeper than 3 cm,

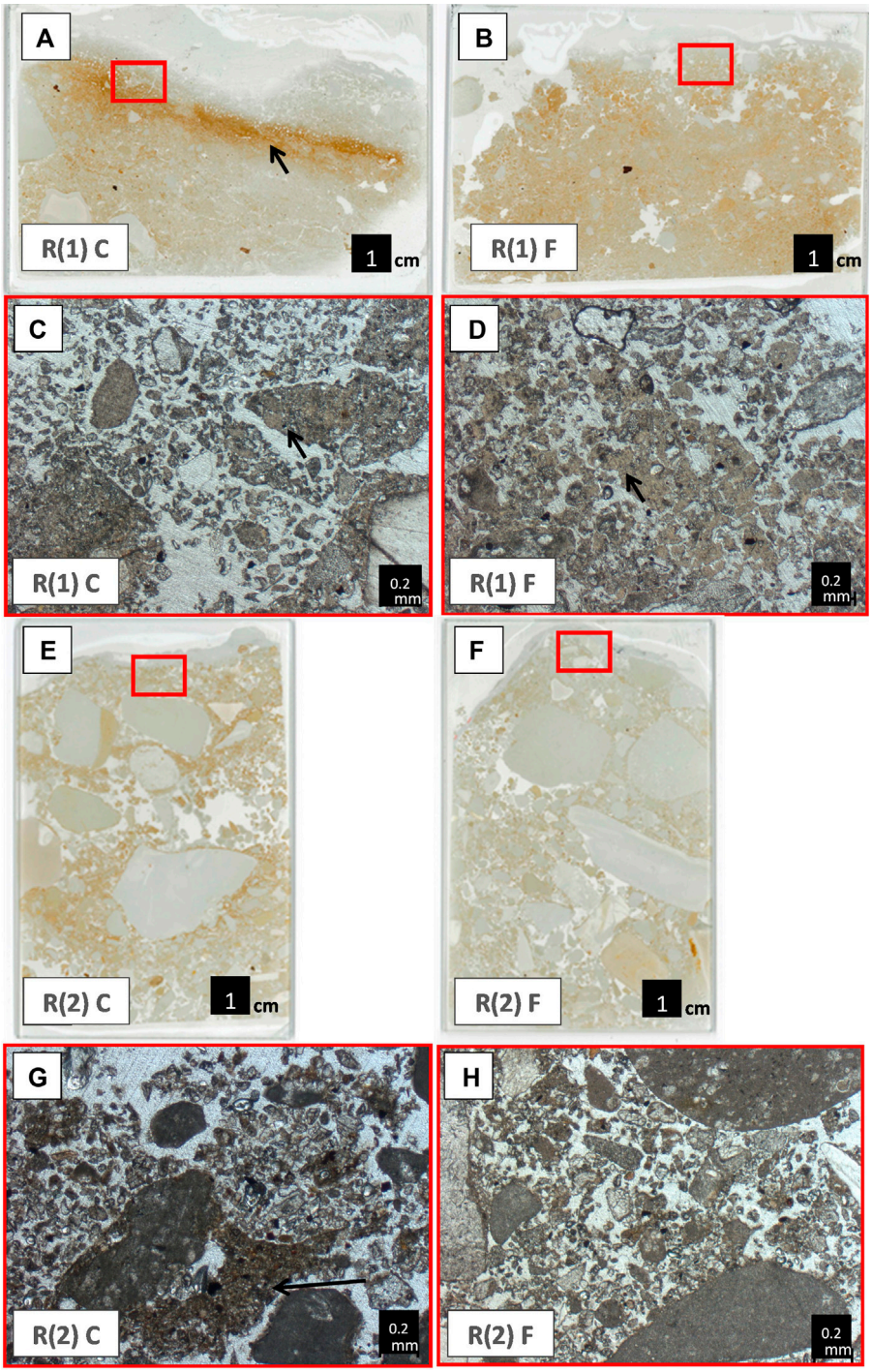


FIGURE 7
Thin section scans and microphotographs (PPL) of the Roman (R) footpath (F) and its control (C) sample in the plane (1) and hillslope (2) sampling locations. Red boxes in the thin section scans indicate the location of microphotographs. **(A)** Scan of non-path control sample R (1), where a silty-clayey desert soil crust layer is marked by an arrow. **(B)** Scan of footpath sample R (1) F. **(C)** An 0.8 mm wide redeposited aggregate serves as evidence of post-depositional activities. **(D)** Cementation and finer aggregates than those of the control sample. **(E)** Scan of non-path control sample R (2) presenting many voids, angular pebbles, indicating the interchanging colluvial-fluvial nature of the accumulation. **(F)** Scan of footpath sample R (2) showing some of the coarser grains following the slope direction which is towards the lower right side of the slide. **(G)** Notice one large clayey-silty bow-like infilling, a bioturbation feature, at the lower part of the micrograph. **(H)** Different sand-sized minerals and a lack of bioturbation or cementation with complex packing voids.

the modern footpath's control sample is less porous than the footpath sample. For all samples, variations along depth in the relative porosity between footpath and control samples are observed and are also partly responsible for the variability within each footpath while incorporating the entire 5 cm (Figure 10A). A trend of relatively increased porosity in the control samples along depth is evident between 0.1–2 cm and then again between 3–5 cm below the surface (Figure 10C).

# 5 Discussion

The surfaces and subsurfaces (ca. 0–15 cm below surface) of the two areas studied in the Judean desert (Figure 1), were previously defined as regolith soil, bare rock and poorly developed lithosol (Steinberger et al., 1999; Singer, 2007). Relating to the nature of accumulation, these are composed of alluvial conglomerate, colluvium and dust (Sneh, 1979; Yechieli et al., 1993; Oldenburg el al., 2000). In order to investigate the interaction between footpaths and the arid natural environment, footpath samples studied here are considered as a "disturbance" to the natural setting examined in three aspects; 1. Changes evident at the surface, in regards to surface-runoff-generation and colors; 2. Changes evident on the subsurface, specifically porosity and pedogenic activity; and 3. Changes through time in relation to long-term use and potential periods of abandonment.

## 5.1 Surface changes

From a mechanical perspective, similar to pathways and footpaths in other environments, footpaths in the Judean Desert show significantly higher penetration resistance than non-path controls (Supplementary Figure S3; Sherman et al., 2019; Nir et al., 2022). Due to the lower porosity and higher surface runoff, footpaths can promote different types of soil erosion (Sutherland et al., 2001; Brandolini et al., 2006; Buchwał and Rogowski, 2010; Sidle et al., 2019; Phillips et al., 2021). Analyzing recreational trails, it has been documented that soil erosion along and outside footpaths is promoted (Studlar, 1980; Ballantyn and Pockering, 2015; Fonseca Filho et al., 2018). Tomczyk and Ewertowski, (2023) recently proposed and illustrated some of the mechanisms behind footpath-related soils erosion, including the dependency of such effects on the location of paths on the slope. Similarly, in the Judean Desert, surface runoff causes soil erosion, in the form of rills and gullies initiating directly downslope from footpaths for both the Roman (2) and the EBA (2) footpath segments, located on hillslopes (Figure 2; Table 1). As evident in other studies, at the watershed level these type of linear soil erosion can contribute to both higher soil loss as well as increase hydraulic connectivity (Sidle et al., 2019; Zgłobicki et al., 2021; Nir et al., 2022).

A second result of footpath trampling is the abrasion of limestone pebbles, exposing its whitish-light colors. The latter interpretation is based on the positive correlation between the green and blue (GB) color bands and calcite content (Figure 5). Another linked factor responsible for the brighter colors on trails is the lower amount of the pure fine grain fraction (silt and clay) on the uppermost cover of the footpath samples, relative to the non-path controls (Figures 5–8; Table 3). The fine fraction was additionally positively correlated with the red (R) color as well as with iron and manganese (Figure 5). Both spectrometer measurements of the fine fractions, as well as RGB values extracted from the UAV orthophotos, show lighter colors on the footpath than on non-path areas. In both scales, the highest degree of change lies in the blue band (Figure 4). This observation could result in up to 5% higher relative brightness or albedo values for the footpaths than for non-path areas (Figure 4). In the nearby Sinai arid peninsula, looking at the opposite effect, increased vegetation cover decreased the albedo values by 25% (Otterman and Tucker, 1985). For a different arid environment, it was suggested that a 2% increase in albedo values can correspond to approximately 2-3°C decrease in surface temperature during spring (Zolotokrylin et al., 2020). Following this analysis, the possible local cooling, resulting from footpaths distributed throughout the Judean Desert over several millennia, should not be underestimated (Efrat, 1993). Looking at the possible effects on the surface, it has been shown that in the arid environment of the southern Levant, soil aggregate stability and biological activities of the surface crust is determined among other factors by temperature (Lavee et al., 1996).

## 5.2 Changes evident in the subsurface

Nir et al. (2022) report that recent and long-term used footpaths in sub-humid clay-silt rich environment and in sandy temperate environment, exhibited changes in pedogenic activities and microstructure in the subsurface, i.e., lower porosity, lower evidence of biogenic remains (O horizon) and higher pedogenic iron oxides in footpaths than in the non-path samples. The proposed mechanism suggested is that lower permeability resulting in 1. Removal of the O horizon through surfaced runoff and soil erosion; and 2. increased water saturation on footpaths surfaces than on non-paths, and in turn, after dehydration, higher amounts of pedogenic iron oxides on footpath surfaces (Nir et al., 2022). In the present study of an arid environment, the Judean Desert, micromorphological differences between the footpaths and their control are less clear. Calcareous-cementation and aggregates found in the modern footpath control sample of the Judean Desert (Table 3; Figures 6C, 9), are the result of seasonal water saturation followed by surface stabilization (Verrecchia et al., 1991; Banfield et al., 1999; Shankar and Achyuthan, 2007). Calcareous-cementation and aggregates in the Judean Desert are likely related to micro-organisms who have played an important role in the formation of both secondary calcite and soil crusts of lithosols and regolith soils. The specific typical biological agents responsible for soil crusts in the Judean Desert are cyanobacteria, fungi, and lichens (Cole, 1990; Steinberger et al., 1999; Sohrabi et al., 2017). Aggregates and calcareous-cementation, observed in the modern footpath control sample, are absent from the corresponding modern footpath sample. Thus, relatively less calcareous matrix and cement, and aggregate formation on the footpath sample, could be interpreted as resulting from a hindrance of the aforementioned surface processes, such as limited water percolation and surface compaction of the footpath. Similar hindrance or degradation of plants and biogenic activities as a result of footpath formation have been documented in other environments (Cole, 2004; Ballantyn and Pockering, 2015; Fonseca Filho et al., 2018; Chenhao et al., 2019; Sherman et al., 2019). While footpath subsurface porosity in the temperate environment is relatively low (compared to controls) throughout a 3 cm depth (Nir et al., 2022), in the Judean Desert, all footpaths show distinct and consistent lower porosity only for the upper 0.1 cm in the thin section (Figure 10). The lower porosity also corresponds to a general trend of higher amounts of fine fractions occupying the voids between the sand grains in footpaths than in control samples (Table 3; Figures 6–8). If the observed differences in footpath porosity ratios between temperate and arid environments are genuine (i.e., not a result of a small sample size, etc.), one explanation for that could be contrasting trampling effects on wet *versus* dry surfaces. Hence, trampling on wet surfaces (i.e., with pores completely filled with water) can result in a higher degree of compaction and lower porosity under footpaths (compared with non-paths), than that resulting from trampling in a dry environment. These interpretations follow similar conclusions reached by other studies addressing soil compaction (Pietola et al., 2005; Botta et al.,

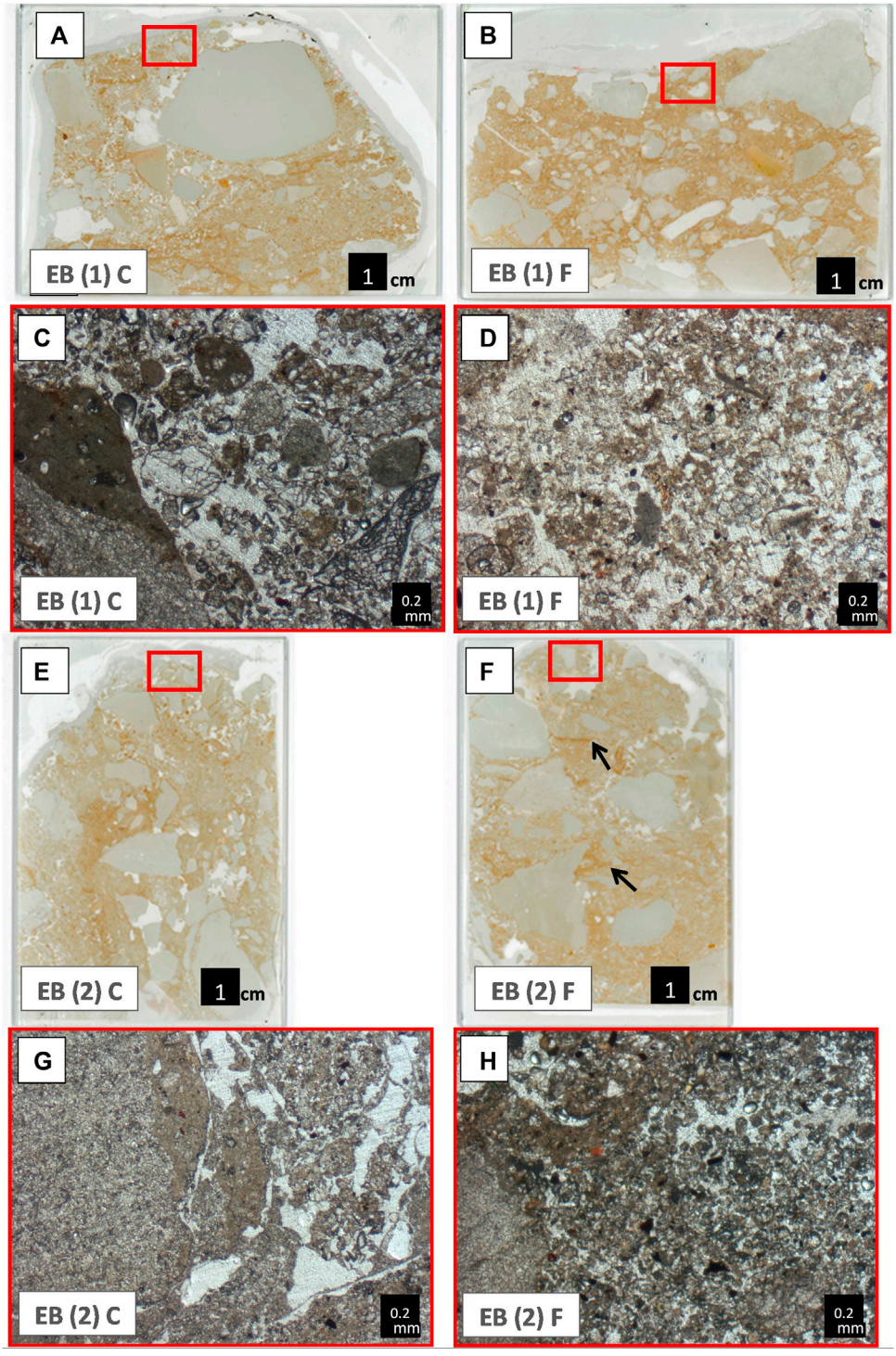


FIGURE 8
Thin section scans and microphotographs (PPL) of the Early Bronze Age (EB) footpath (F) and its control (C) sample, directly below the saddle (1) and on the hillslope (2) sampling locations. Red boxes in the thin section scans indicate the location of microphotographs. **(A)** Scan of non-path control sample EB (1) showing gravel sized grains on the upper layer while at 4 cm below surface, fine-grained sediments are more abundant. **(B)** Scan of footpath sample EB (2) exhibiting a homogenous distribution of fine gravel throughout the slide. **(C)** Rounded medium and large sands and poorly sorted grain sizes, suggesting colluvial origins. **(D)** Notice brown-dark organic features and iron/manganese oxide nodules. **(E)** Scan of non-path control sample EBA (2) showing a colluvial nature of the deposit indicated by angular pebbles positioned in a semi-vertical orientation. **(F)** Scan of footpath sample EBA (2) with well-preserved but truncated slacking crusts marked with arrows. **(G)** Gravel and calcareous cementing material. **(H)** Massive microstructure and brown-dark organic features and iron/manganese oxide nodules.

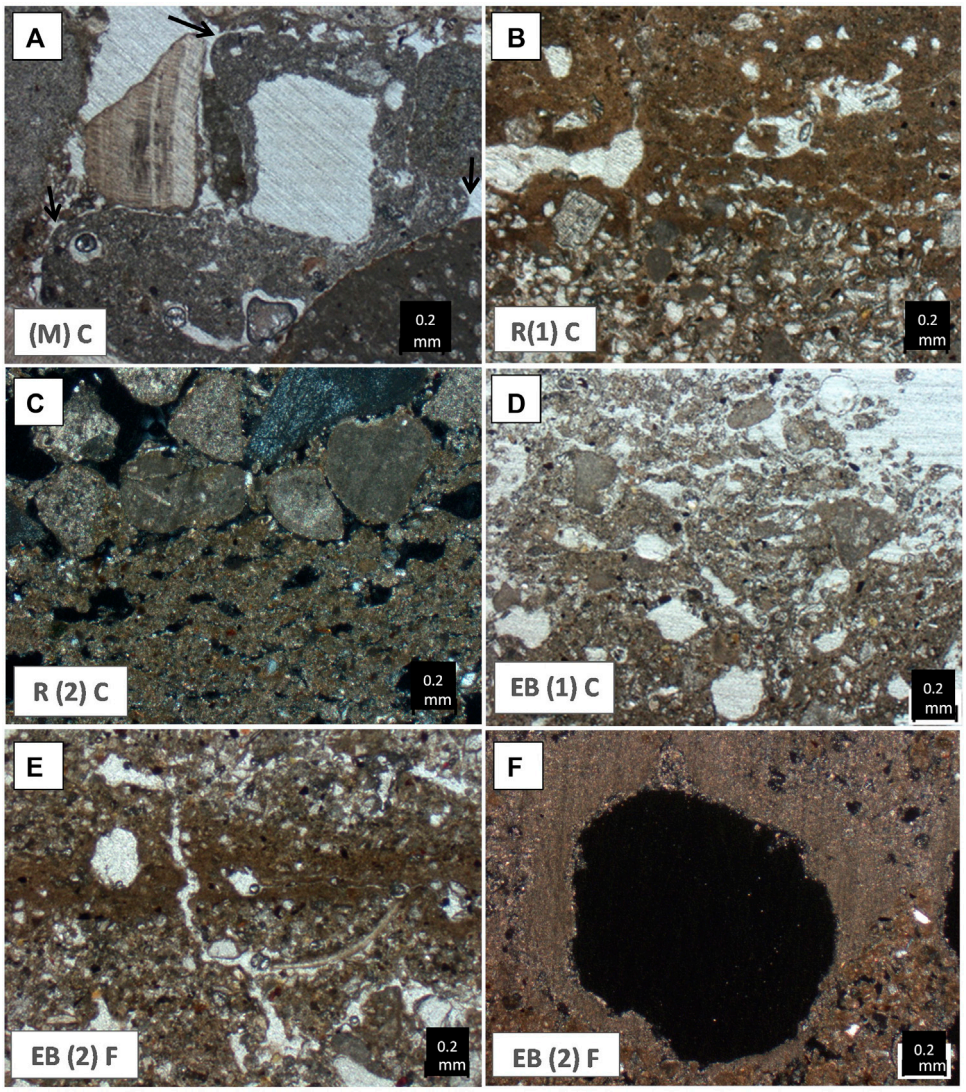


FIGURE 9
Microphotographs of selected samples (PPL unless mentioned otherwise) showing bio-and pedo-genic processes under the different footpaths, and control samples. Control samples: **(A)** Calcareous cement/matrix with irregular rounded edges (biogenic/plant activity) in non-path control sample (M). **(B)** Vughy structure on the contact between a slaking crust layer and a coarser unit in Roman non-path control sample (R (1). **(C)** Vesicles ina biogenic matrix in non-path control sample (R (2) (XPL). **(D)** Channels and interconnected vesicles and vughs in micritic matrix in EBA non-path control sample (EB (1). Footpath samples: **(E)** Channel/vesicles and vertical plane in a slacking crust in EBA footpath sample (EB (2). **(F)** Cross-section of a large channel with a calcareous (quasi) coating in EBA footpath sample (EBA (2) (XPL).

2020). For the Roman footpath segment sampled in the plane area, the control sample shows clear surface and pedogenic activities which includes a 1 cm thick, horizontal clayey microlayer with vesicles as well as aggregates. In the footpath sample, no such clay layer is present while mechanical compaction is evident. However, some pedogenic activities in the footpath sample are suggested by calcareous cementation, likely the result of plant roots. For the same Roman footpath, but sampled on the hillslope, the control sample shows channels and transported aggregates, representing low energy depositions and bioturbation. Contrastingly, the footpath sample, while also representing colluvium, shows no clear indications of bioturbation. This may be due to both the reduction in surface water stagnation and availability resulting from trampling that would in turn reduce biogenic activities but also, though less likely, due to homogenization by trampling that would mask any indication of bioturbation that already occurred. For both EBA footpath samples, also from slope contexts, a general matrix supported and homogenized microstructure of the uppermost ca. 1 cm was observed. In their non-footpath controls however, we, observed a more grain supported microstructure in the uppermost 1 cm (Table 3; Figures 8, 9). Further indicators, such as decrease in bioturbation and aggregates, which form a distinct difference between control and footpath samples for footpaths in the plane areas, were not evident or very minor for the footpaths on the hillslopes. The colluvial processes on those hillslopes would encourage the removal of surface sediments. Following that notion, it has long been shown for the southern Levant arid regions that decreased soil cover on slopes would result in lower water permeability and soil biogenic activities while generating high surface runnoff which would be especially true for the EBA hillslope (Yair, 1990).

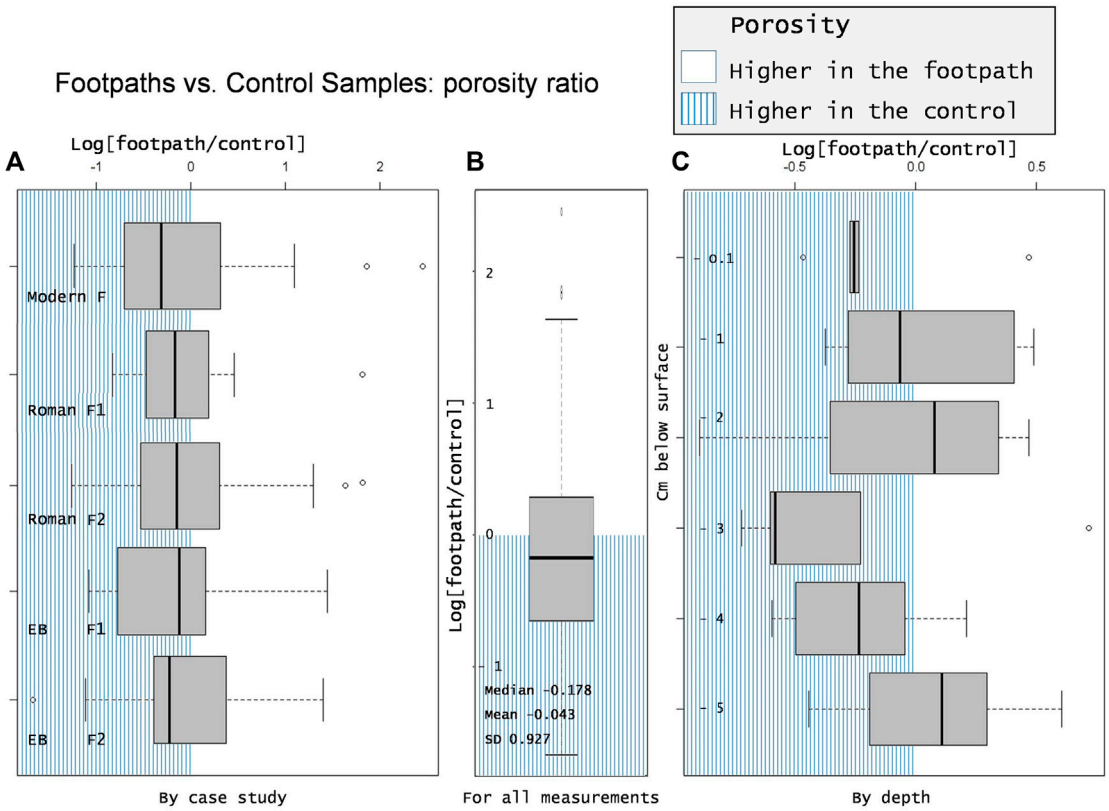


FIGURE 10
Porosity ratios of footpaths and their corresponding control samples (log (footpath/control) along 5 cm for each micromorphological slide. Presented according to **(A)**. The individual paths, **(B)**. Combined and **(C)**. By depth ($n$ = 180, at 0.1 and 3 cm below the surface: $p<0.05$ otherwise: $p>0.05$).

## 5.3 Long-term used footpaths

Absolute dating methods (e.g., radiocarbon dating, Optical Stimulated Luminesce (OSL), Beryllium-10) are routine techniques in establishing a time of deposition for both archaeological sites, sediments exposures and sediment cores (Rodríguez-Rodríguez et al., 2014; Roberts et al., 2015; Boaretto et al., 2021). However, for several centimeters of subsurface, laying outside clear archaeological context, these methods are challenging to apply. Conducting absolute dating in such context is especially challenging due to the limited datable subsurface material in arid environments, as well as to the interpretation of such materials as part of the early use of a footpath (Langgut et al., 2014). However, most control and footpath samples studied here, include silt to sand sized quartz and in some cases mica grains, suggesting a continues aeolian input in the Zohar Ascent and in the Wadi Zeelim outlet, or for the latter, reworked aeolian deposition originating from the Negev highlands (Sneh, 1979; Singer, 2007; Roskin et al., 2017). Such grains may prove as useful for future OSL measurements. Having stated that, in various environments, assessing the date of pathways and roads have often been established using dating from archaeological sites along the roads or on the basis of travel waste and historical evidence (Aharoni and Rothenebrg, 1960; Zedeño and Stoffle, 2003; Davidovich, 2014; Sidebotham et al., 2019). In the curent study we relay on a series of survey finds including installations and movement waste on the surface attributed to the Roman period, and similar finds and nearby excavations attributed to the Early Bronze Age, that have resulted in the affiliation of use of two of the studied footpaths to these times (Yekutieli, 2005; 2006; Davidovich, 2014). Therefore, the Early Bronze Age and the Roman period are regarded here as dominant phases within the lifespan of the two archaeologically attributed footpaths. Subsequently, any later (including recent) use of these trails could not be excluded, as recurrent use of existing trail systems is a well-known phenomenon (Jackson, 1994). Hence, we consider these two footpaths to be under long-term use during the Holocene, rather than proclaiming their absolute formation only to the specified archaeological periods.

Geomorphologically, the relative antiquity of the footpaths could be assessed through the interaction between linear soil erosion and the location of trails (Watchman and Twidale, 2002). On the plane area of the Wadi Zeelim outlet, the current streambed truncates the Roman footpath (1), indicating that the path predates the current riverbed configuration (Figure 3). It is worth noting that in the Judean Desert, within areas that are no longer fluvially active, such as hillslopes and elevated planes, certain pedogenic and fluvial processes are minimal, at times allowing better preservation of archaeological remains (Fanning et al., 2009). In contrast, active Wadi riverbeds in the Judean Desert can quickly incise and undercut the sedimentary accumulation due to the high surface runoff and the subsequently intense floods, as well as the decline in the levels of the Dead Sea. On the hillslope area of the Zeelim Wadi, some gullies and rills, or their outlets, overlie parts of the Roman footpath (2), Similarly, suggesting the latter predates the former (Figure 3). Hence, these features further imply a minimal recent-modern use of the Roman period footpath, but without absolute

dating the geomorphological evidence is highly circumstantial (Watchman and Twidale, 2002).

For the long-term used trails studied here (affiliated with the EBA and Roman period), the only consistent differences evident between the modern footpath sample and their control is the increased compaction of the sediments under footpaths, compared with the control samples (Table 3; Figures 6–8, 10). Beyond that, for the long-termed used footpaths, no micro-archaeological remains of their use were found and we observed no other consistent (post)depositional markers. Instead, differences are context specific. For the Roman footpath segment sampled in the plane area, the minor calcareous cementation resulting from plant roots activities may reflect on periods of abandonment of the path as also evident from the current stream bed cutting the footpaths' course and preventing passage. Such abandonment could result in a slight increase in porosity and water saturation followed by plant growth. Considering that dryland bacterial communities can recover within years of the original disturbance, such recovery cannot be overruled (Cole, 1990; Steven et al., 2021). For the EBA footpaths, multiple slacking crusts suggesting some degree of water saturation (e.g., puddle) as well as calcareous cementation, indicating post-depositional activities, were evident in both footpath (EBA (2) and control samples (EBA (1). These crusts do not exhibit granular structure which would suggest there were affected by trampling (Stahlschmidt et al., 2019). The likely abandonment of these route, based on archaeological evidence, directly after the Bronze Age may have resulted in over four millennia of potential recuperation, in which case the footpath surfaces would act more similar to non-path controls, including the formation of non granular slacking crusts (Yekutieli, 2005; 2006; Davidovich, 2014).

## 5.4 Method evaluation

Four methods were used to identify and assess the overall sediment and soil characters of ancient and modern footpaths in arid contexts. Analysing bulk parameters such as pH and electric conductivity as well as Cl-, intended to identify soil forming processes such as organic decay (Öberg, 1998), salt dislocation and evaporation (Mabbutt, 1977; McFadden and Knuepfer, 1990), as well as possible clay lessivage (Khormali and Abtahi, 2003) while overall grain size analysis provided the textural picture required for a valid process understanding (Kettler et al., 2001). Unfortunately, the analysis of these (bulk) parameters (i.e., grain size, pH, EC, elemental) did not allow differentiation of samples originating from footpaths and non-footpaths (Supplementary Figure S1). However, this lack of differentiation might be the result of the sampling strategy extracting bulk-samples of 5-cm thickness (0–5 cm depth, 5–10 cm depth, 10–15 cm depth) not allowing a high resolution of near surface material characters by lab parameters, while in parallel the micromorphological thin sections allow a high resolution analysis of the material regarding structure and texture (Figure 5). In consequence, a sampling strategy with higher resolution such as <1 cm intervals could prove itself as useful (Giesler and Lundström, 1993; Wells, 2010). Using micromorphology, a hindrance of pedogenic activities under the modern footpath sampled in the plane area compared with its control was observed while archaeologically affiliated footpaths, in the hill slope areas in particular, showed greater variability and no clear trend was observed beyond surface compaction (Figures 6–9). Due to the variable micromorphological observations between samples, e.g., the occurrence of slaking crusts, calcareous cementation and the degree of bioturbation, a larger sample set that includes spatially diverse contexts would be necessary to validate these trends (Croix et al., 2019). Furthermore, the integration of the micromorphological sampling with stratigraphic observations in such "test pit excavations" of a footpath, would require more intense field documentation of the complete path with multiple pits/trenches to better follow the stratigraphy of the path and non-path areas and test their change across various micro-environments. For both the Roman and EBA affiliated trails, an important constraint in our ability to identify a historical trail could lie in the interpretation of abandoned ancient footpaths as opposed to less frequently used modern footpaths. The former may have similar micro-features to the latter. However, it has been shown that after two dozen events of footpath trampling, the fresh soil crust layers are destroyed (Cole, 1990). This implies that minimally used recent footpaths should bear, to some extent, similarities to the intensely used modern trails rather than to ancient trails, if used concurrently. Image analysis has long been used in a micromorphological context, including attempts at assessing the degree of porosity (Pires et al., 2009). In some cases, such analysis included the successful estimation of void types. However, comparing the results of different case studies and authors to assess the degree of porosity is challenging as authors use different softwares, many times not accessible to others (Rasa et al., 2012). Using image analysis in an open-source R environment to evaluate subsurface porosity has produced a result showing a significant reduction of porosity in footpath samples compared with non-path controls at 0.1 cm below the surface alone (Figure 10) in agreement with surface penetration resistance measurements. In more humid environments the significantly lower porosity reached 3 cm below the surface, suggesting that this tool could be useful for comparing between environments (Nir et al., 2022). Using UAV and laboratory analysis for assessing color differences between footpaths and non-footpaths is very insightful (Figure 4). Coupled with elemental and grain size analyses (Figure 5), the combination of these results was helpful for understanding the contribution of abraded larger (sands, gravels, pebbles) grains to the resulting bright color of footpaths while iron rich silts and clays (dominating the undisturbed control areas) correlate with the darker red color (Chase et al., 2012). Therefore, using UAV, laboratory analysis and surface penetration resistance could prove itself useful for footpath recognition. Additionally, with a larger and well-contextualized sample set, detailed micromorphological analysis can evaluate formation processes related to footpath use and, again context- and analogy-dependent, whether the path could have been used in the long-term or abandoned. This could be especially true for footpaths located in arid-environments on plane areas, where water accumulate seasonally during flooding events, resulting in an overall similar depositional and bio/pedogenetic processes to the subsurface. The latter processes would be then more recognizable and their hindering easier to differentiate by the formation of footpaths.

# 6 Conclusion

In this paper we studied three footpaths in the arid environment of the Judean Desert of variable temporal contexts, representing recent and long-term, including archaeological use. The interstratification of the footpaths with geomorphological features, resulting, for example from

gully erosion or river incising, served as relative indicators for the antiquity of a trail and in concert with the occurrence of archaeological remains (from different epochs) suggests that these trails have been active through a long time period. On the other hand, gullies initiating from footpaths bear witness to the local geomorphological impact of footpaths. Our analysis shows a general trend of increased compactness, lower porosity, and brighter colors in the footpaths compared to their immediate surroundings and controls. For the high-resolution UAV data, footpaths have a significantly higher albedo value than the non-trail surrounding areas. Using micromorphology, the main consistent difference is increased compaction of the sediments in footpaths compared to the controls while a few variable proxies, i.e., bioturbation, water percolation and homogenization of the sediments seem to be effected by footpath formation, however, their occurrence and expression varies by slope angel and archaeological context and they are more difficult to explain. Modern footpath sample shows the most striking examples of the above mentioned differences (e.g., open microstructure, calcareous cementation, slacking crust and vesicles in the control sample but not in the footpath), while the archaeological trails present mixed trends. This is could be due to micro-environmental variability, slope angle, and time passed since its intense usage and suggested abandonment. Looking at signals related to these processes, a differentiation between modern and archaeological trails based on qualitative micromorphology was not straightforward. Beyond, higher penetration resistance and thin section lower-porosity is evident in footpath near surfaces for the studied arid environment. However, in the arid zone porosity is significantly lower than corresponding controls only 0.1 cm below the surface while in previously studied temperate zone, relative porosity is lower down to 3 cm below the surface. This supports other studies that suggested that trampling on wet surfaces results in a higher degree of compaction than on dry ones. By sampling in multiple locations and using well defined controls, a combination of R based porosity analysis and micromorphological description can be used as tools for supporting archeological endeavors in uncovering (pre)historical footpaths. Further investigation using UAV and color recognition could be useful to explore the distribution of trails, particularly in arid limestone environments, as such effect could emerge as one of the earliest types of human-made (micro)climate change. A remote sensing approach could possibly quantify the albedo effect that ancient and modern trails hold on the landscape.

## Data availability statement

The datasets presented in this study can be found in online repositories. The names of the repository/repositories and accession number(s) can be found in the article/Supplementary Material.

## Author contributions

NN–Geo-and micro-morphological conceptualization, data collection and analysis. UD–Archaeological framework conceptualization and data collection MU–Archaeological framework conceptualization and data collection BS–Geomorphological conceptualisation and supervision MS–Micromorphological conceptualization, data analysis and supervision. All authors contributed to the article and approved the submitted version.

## Acknowledgments

We would like to thank Moritz Nykamp, Philipp Hoelzmann, and René Schatten from the laboratory for Physical Geography at the Freie Universität Berlin and to Catrin Vetter from the Julius Kühn-Institut. Continued support was given by Jacob Hardt, Robert Busch, and the PhD students and postdocs of the Physical Geography working group at FU Berlin. Special thanks to Ruth Shahack Gross from Haifa University and Ariel Malinsky Buller of the Hebrew University of Jerusalem and Anna Shraer. Thanks also to the Studienstiftung des Deutschen Volkes for personal funding during this research period. We thank the reviewers for improving this manuscript.

## Conflict of interest

The authors declare that the research was conducted in the absence of any commercial or financial relationships that could be construed as a potential conflict of interest.

## Publisher's note



## Supplementary material

The Supplementary Material for this article can be found online at: https://www.frontiersin.org/articles/10.3389/feart.2023.1148101/full#supplementary-material

## References

Aharoni, Y., and Rothenebrg, B. (1960). *In the foosteps of kings and rebels in the Judean desert*. Tel Aviv: Massada.

Amiran, R., and Ilan, O. (1978). *Early Arad: The chalcolitic settlement and early bronze city*.

Ayers, E., Nkem, J. N., Wall, D. H., dams, B. J., Barrett, J. E., Broos, E. J., et al. (2008). Effects of human trampling on populations of soil fauna in the McMurdo Dry Valleys, Antarctica. *Conservation Biol. J. Soc. Conservation Biol.* 22, 1544–1551. doi:10.1111/j.1523-1739.2008.01034.x

Ballantyn, M., and Pockering, C. M. (2015). The impacts of trail infrastructure on vegetation and soils: current literature and future directions. *J. Environ. Manag.* 164, 53–64. doi:10.1016/j.jenvman.2015.08.032

Banfield, J. F., Barker, W. W., Welch, S. A., and Taunton, A. (1999). Biological impact on mineral dissolution: application of the lichen model to understanding mineral weathering in the rhizosphere. *Proc. Natl. Acad. Sci.* 96 (7), 3404–3411. doi:10.1073/pnas.96.7.3404

Bar-Yosef, O. (1986). The walls of Jericho: an alternative interpretation. *Curr. Anthropol.* 27, 157–162. doi:10.1086/203413

Blum, P. (1997). *Physical properties handbook: A guide to the shipboard measurement of physical properties of deep-sea cores*.

Boardman, J. (2022). Sunken lanes in southern england: A review. *Proc. Geologists' Assoc.* 133, 481–490. doi:10.1016/j.pgeola.2022.06.001

Boaretto, E., Hernandez, M., Goder-Goldberger, M., Aldeias, V., Regev, L., Caracuta, V., et al. (2021). The absolute chronology of boker tachtit (Israel) and implications for the middle to upper paleolithic transition in the levant. *Proc. Natl. Acad. Sci.* 118 (25), e2014657118. doi:10.1073/pnas.2014657118

Boelhouwers, J., and Scheepers, T. (2004). The role of antelope trampling on scarp erosion in a hyper-arid environment, Skeleton Coast, Namibia. *J. arid Environ.* 58, 545–557. doi:10.1016/j.jaridenv.2003.11.006

Botta, G. F., Antille, D. L., Bienvenido, F., Rivero, D., Avila-Pedraza, E. A., Contessotto, E. E., et al. (2020). Effect of cattle trampling and farm machinery traffic on soil compaction of an Entic Haplustoll in a semiarid region of Argentina. *Agron. Res.* 18, 1163–1176. doi:10.15159/ar.20.063

Brandolini, P., Faccini, F., and Piccazzo, M. (2006). Geomorphological hazard and tourist vulnerability along portofino park trails (Italy). *Nat. Hazards Earth Syst. Sci.* 6, 563–571. doi:10.5194/nhess-6-563-2006

Buchwał, a., and Rogowski, M. (2010). The methods of preventing trail erosion on the examples of intensively used footpaths in the tatra and the babia góra national parks. *Geomorphol. Slovaca Bohemica* 10, 7–15.

Cao, C., Lee, X., Muhlhausen, J., Bonneau, L., and Xu, J. (2018). Measuring landscape albedo using unmanned aerial vehicles. *Remote Sens.* 10, 1812. doi:10.3390/rs10111812

Charbonnier, M.-c., and Cammas, C. (2018). Characterization of gallo-roman roads in northern France using micromorphological methods. *Quat. Int.* 483, 194–210. doi:10.1016/j.quaint.2018.05.010

Chase, a. F., Chase, D. Z., Fisher, C. T., Leisz, S. J., and Weishampel, J. F. (2012). Geospatial revolution and remote sensing lidar in mesoamerican archaeology. *Proc. Natl. Acad. Sci.* 109, 12916–12921. doi:10.1073/pnas.1205198109

Chenhao, X., Longtang, L., and Jie, R. (2019). Response and simulation of vegetation in desert scenic spot to tourists' trampling disturbance. *Cross-cultural Commun.* 15, 15–24. doi:10.3968/11426

Cole, D. N. (2004). Impacts of hiking and camping on soils and vegetation: A review. *Environ. Impacts Ecotourism* 41, 60.

Cole, D. N. (1990). Trampling disturbance and recovery of cryptogamic soil crusts in grand canyon national park. *Gt. Basin Nat.*, 321–325.

Courty, M. A., Goldberg, P., and Macphail, R. (1989). *Soils and micromorphology in archaeology*. Cambridge: Cambridge.

Croft, D. B. (2019). Walking in each other's footsteps: do animal trail makers confer resilience against trampling tourists? *Environments* 6, 83. doi:10.3390/environments6070083

Croix, S., Deckers, P., Feveile, C., Knudsen, M., Qvistgaard, S. S., Sindbæk, S. M., et al. (2019). Single context, metacontext, and high definition archaeology: integrating new standards of stratigraphic excavation and recording. *J. Archaeol. Method Theory* 26, 1591–1631. doi:10.1007/s10816-019-09417-x

Davidovich, U. (2013). *The chalcolithic-early bronze age transition: A view from the Judean Desert caves, southern levant*. Paléorient, 125–138.

Davidovich, U. (2014). *The Judean Desert during the chalcolithic, bronze and iron ages (Sixth–first millennia bce): Desert and sown relations in light of activity patterns in a defined desert environment*.

Efrat, E. (1993). Human ecology and the albedo effect in an arid environment. *Hum. Ecol.* 21, 281–293. doi:10.1007/bf00891540

Eichhorn, B., Hendrickx, S., Riemer, H., and Stern, B. (2005). Desert roads and transport vessels from late roman-Coptic times in the eastern sahara. *J. Afr. Archaeol.* 3, 213–229. doi:10.3213/1612-1651-10051

Eldridge, D. J. (1998). Trampling of microphytic crusts on calcareous soils, and its impact on erosion under rain-impacted flow. *Catena* 33, 221–239. doi:10.1016/s0341-8162(98)00075-7

Fanning, P. C., Holdaway, S. J., Rhodes, E. J., and Bryant, T. G. (2009). The surface archaeological record in arid Australia: geomorphic controls on preservation, exposure, and visibility. *Geoarchaeology Int. J.* 24 (2), 121–146. doi:10.1002/gea.20259

Foley, R. A., and Lahr, M. M. (2015). Lithic landscapes: early human impact from stone tool production on the central saharan environment. *Plos One* 10, E0116482. doi:10.1371/journal.pone.0116482

Fonseca Filho, R. E., Varajão, a. F. D. C., Figueiredo, M. D. A., and Castro, P. D. T. A. (2018). Pedological aspects as environmental quality indicators of a touristic trail in the serra do cipó national park/mg. *Rem-international Eng. J.* 71, 543–551. doi:10.1590/0370-44672016710123

Garfunkel, Z., and Ben-avraham, Z. (1996). The structure of the Dead Sea basin. *Tectonophysics* 266, 155–176. doi:10.1016/s0040-1951(96)00188-6

Gibling, M. R. (2018). River systems and the anthropocene: A late Pleistocene and Holocene timeline for human influence. *Quaternary* 1, 21. doi:10.3390/quat1030021

Giesler, R., and Lundström, U. (1993). Soil solution chemistry: effects of bulking soil samples. *Soil Sci. Soc. Am. J.* 57, 1283–1288. doi:10.2136/sssaj1993.03615995005700050020x

Goldberg, P., and Macphail, R. (2008). *Practical and theoretical geoarchaeology*. Oxford: Blackwell Publishing.

Goldberg, P. (2018). *Micromorphology*. The Encyclopedia of Archaeological Sciences, 1–4.

Gutiérrez-rodríguez, M., Lechuga Chica, M. Á., Moreno Padilla, M. I., and Bellón Ruiz, J. P. (2022). Microstratigraphic analysis of the main roman road in hispania: the via augusta where it passes through the ianus augustus (mengíbar, Spain). *Archaeol. Anthropol. Sci.* 14, 142–232. doi:10.1007/s12520-022-01602-6

Hardt, J., Nir, N., Lüthgens, C., Menn, T. M., and Schütt, B. (2023a). Palaeoenvironmental research at hawelti-melazo (tigray, northern Ethiopia) – insights from sedimentological and geomorphological analyses. *E&g Quat. Sci. J.* 72, 37–55. doi:10.5194/egqsj-72-37-2023

Hardt, J., Nir, N., and Schütt, B. (2023b). Combining historical maps, travel itineraries and least-cost path modelling to reconstruct pre-modern travel routes and locations in northern tigray (Ethiopia). *Cartogr. J.*, 1–17. doi:10.1080/00087041.2022.2150363

Jackson, J. B. (1994). *A sense of place, a sense of time*. Yale University Press.

Jackson, J. B. (1984). *Discovering the vernacular landscape*. Yale University Press.

Kettler, T. A., Doran, J. W., and Gilbert, T. L. (2001). Simplified method for soil particle-size determination to accompany soil-quality analyses. *Soil Sci. Soc. Am. J.* 65 (3), 849–852. doi:10.2136/sssaj2001.653849x

Khormali, F., and Abtahi, A. (2003). Origin and distribution of clay minerals in calcareous arid and semi-arid soils of Fars Province, southern Iran. *Clay Miner.* 38 (4), 511–527. doi:10.1180/0009855023740112

Langgut, D., Neumann, F. H., Stein, M., Wagner, a., Kagan, E. J., Boaretto, E., et al. (2014). Dead Sea pollen record and history of human activity in the judean highlands (Israel) from the intermediate Bronze into the iron ages (~2500–500 BCE). *Palynology* 38, 280–302. doi:10.1080/01916122.2014.906001

Lavee, H., Sarah, P., and Imeson, a. (1996). Aggregate stability dynamics as affected by soil temperature and moisture regimes. *Geogr. Ann. Ser. a, Phys. Geogr.* 78, 73–82. doi:10.1080/04353676.1996.11880453

Liddle, M. J. (1975). A selective review of the ecological effects of human trampling on natural ecosystems. *Biol. Conserv.* 7, 17–36. doi:10.1016/0006-3207(75)90028-2

Lisker, S., Porat, R., and Frumkin, a. (2010). Late neogene rift valley fill sediments preserved in caves of the Dead Sea fault escarpment (Israel): palaeogeographic and morphotectonic implications. *Sedimentology* 57, 429–445. doi:10.1111/j.1365-3091.2009.01089.x

Loor, I., and Evans, J. (2021). Understanding the value and vulnerability of informal infrastructures: footpaths in quito. *J. Transp. Geogr.* 94, 103112. doi:10.1016/j.jtrangeo.2021.103112

Mabbutt, J. A. (1977). *Desert landforms*. Australian National University Press.

Malinsky-buller, a., Glauberman, P., Ollivier, V., Lauer, T., Timms, R., Frahm, E., et al. (2021). Short-term occupations at high elevation during the middle paleolithic at kalavan 2 (republic of Armenia). *Plos One* 16, E0245700. doi:10.1371/journal.pone.0245700

McFadden, L. D., and Knuepfer, P. L. (1990). Soil geomorphology: the linkage of pedology and surficial processes. *Geomorphology* 3 (3-4), 197–205. doi:10.1016/0169-555x(90)90003-9

Miller, C. E., Conard, N. J., Goldberg, P., and Berna, F. (2010). *Dumping, sweeping and trampling: Experimental micromorphological analysis of anthropogenically modified combustion features*.

Nicosia, C., and Stoops, G. (2017). *Archaeological soil and sediment micromorphology*. John Wiley and Sons.

Nir, N., Stahlschmidt, M., Busch, R., Lüthgens, C., Schütt, B., and Hardt, J. (2022). Footpaths: pedogenic and geomorphological long-term effects of human trampling. *Catena* 215, 106312. doi:10.1016/j.catena.2022.106312

Nykamp, M., Knitter, D., and Schütt, B. (2020). Late Holocene geomorphodynamics in the vicinity of göbekli tepe, Se Turkey. *Catena* 195, 104759. doi:10.1016/j.catena.2020.104759

Öberg, G. (1998). Chloride and organic chlorine in soil. *Acta hydrochimica hydrobiologica* 26 (3), 137–144. doi:10.1002/(sici)1521-401x(199805)26:3<137::aid-aheh137>3.0.co;2-1

Oldenburg, T. B., Rullkötter, J., Böttcher, M. E., and Nissenbaum, A. (2000). Molecular and isotopic characterization of organic matter in recent and sub-recent sediments from the Dead Sea. *Org. Geochem.* 31 (4), 251–265. doi:10.1016/s0146-6380(00)00015-2

Otterman, J., and Tucker, C. (1985). Satellite measurements of surface albedo and temperatures in semi-desert. *J. Appl. Meteorology Climatol.* 24, 228–235. doi:10.1175/1520-0450(1985)024<0228:smosaa>2.0.co;2

Phillips, J. D., Marion, D. A., and Kilcoyne, K. G. (2021). Fine sediment storage in an eroding forest trail system. *Phys. Geogr.* 42, 50–72. doi:10.1080/02723646.2020.1743613

Pietola, L., Horn, R., and Yli-halla, M. (2005). Effects of trampling by cattle on the hydraulic and mechanical properties of soil. *Soil Tillage Res.* 82, 99–108. doi:10.1016/j.still.2004.08.004

Pires, L. F., Reichardt, K., Cooper, M., Cássaro, F. A., Dias, N. M. P., and Bacchi, O. O. S. (2009). Pore system changes of damaged Brazilian oxisols and nitosols induced by wet-dry cycles as seen in 2-d micromorphologic image analysis. *An. Da Acad. Bras. De. Ciências* 81, 151–161. doi:10.1590/s0001-37652009000100016

R Core Team, R. (2013). *R: A language and environment for statistical computing*.

Rasa, K., Eickhorst, T., Tippkötter, R., and Yli-halla, M. (2012). Structure and pore system in differently managed clayey surface soil as described by micromorphology and image analysis. *Geoderma* 173-174, 10–18. doi:10.1016/j.geoderma.2011.12.017

Rast, W. (2001). *Early bronze age state formation in the southeast Dead Sea plain, Jordan. Studies in the archaeology of Israel and neighboring lands in memory of douglas L. Esse*, 519–533.

Rentzel, P., Nicosia, C., Gebhardt, a., Brönnimann, D., Pümpin, C., and Ismail-meyer, K. (2017). *Trampling, poaching and the effect of traffic*. Archaeological Soil and Sediment Micromorphology, 476.

Roberts, R. G., Jacobs, Z., Li, B., Jankowski, N. R., Cunningham, A. C., and Rosenfeld, A. B. (2015). Optical dating in archaeology: thirty years in retrospect and grand challenges for the future. *J. Archaeol. Sci.* 56, 41–60. doi:10.1016/j.jas.2015.02.028

Rodway-dyer, S., and Ellis, N. (2018). Combining remote sensing and on-site monitoring methods to investigate footpath erosion within a popular recreational heathland environment. *J. Environ. Manag.* 215, 68–78. doi:10.1016/j.jenvman.2018.03.030

Rodríguez-Rodríguez, L., Jiménez-Sánchez, M., Domínguez-Cuesta, M. J., Rinterknecht, V., Pallàs, R., Bourlès, D., et al. (2014). A multiple dating-method approach applied to the Sanabria Lake moraine complex (NW Iberian Peninsula, SW Europe). *Quat. Sci. Rev.* 83, 1–10. doi:10.1016/j.quascirev.2013.10.019

Rodway-dyer, S., and Walling, D. (2010). The use of 137cs to establish longer-term soil erosion rates on footpaths in the UK. *J. Environ. Manag.* 91, 1952–1962. doi:10.1016/j.jenvman.2010.04.014

Roskin, J., Bookman, R., Friesem, D. E., and Vardi, J. (2017). A late Pleistocene linear dune dam record of aeolian-fluvial dynamics at the fringes of the northwestern Negev dunefield. *Sediment. Geol.* 353, 76–95. doi:10.1016/j.sedgeo.2017.03.011

Salesa, D., and Cerdà, a. (2020). Soil erosion on mountain trails as a consequence of recreational activities. A comprehensive review of the scientific literature. *J. Environ. Manag.* 271, 110990. doi:10.1016/j.jenvman.2020.110990

Schild, a. (2016). *Archaeological least Cost path modeling: A behavioral study of middle bronze age merchant travel routes across the amanus mountains, Turkey*. University of Southern California.

Schulten, a., Lammerer, a., Paulsen, R., Regling, K., and Schramm, E. (1933). *Masada die burg des herodes und die römischen lager mit einem anhang: Beth-ter*. Zeitschrift Des Deutschen Palästina-vereins 1878-1945, 1–185.

Shankar, N., and Achyuthan, H. (2007). Genesis of calcic and petrocalcic horizons from coimbatore, Tamil nadu: micromorphology and geochemical studies. *Quat. Int.* 175 (1), 140–154. doi:10.1016/j.quaint.2007.05.017

Sherman, C., Unc, a., Doniger, T., Ehrlich, R., and Steinberger, Y. (2019). The effect of human trampling activity on a soil microbial community at the oulanka natural reserve, Finland. *Appl. Soil Ecol.* 135, 104–112. doi:10.1016/j.apsoil.2018.11.013

Sidebotham, S. E., Gates-Foster, J., Rivard, J. L. G., Wright, H. T., and Tomber, R. (2019). *The archaeological survey of the desert roads between Berenike and the Nile valley*. Boston: American Schools of Oriental Research, 73.

Sidle, R. C., Jarihani, B., Gallant, J., and Koci, J. (2019). *Evidence of how roads and trails contribute to gully erosion in drylands*.

Singer, a. (2007). *The soils of Israel*. Springer Science and Business Media.

Sneh, A. (1979). Late Pleistocene fan-deltas along the Dead Sea Rift. *J. Sediment. Res.* 49 (2), 541–551.

Sohrabi, M., Favero-Longo, S. E., Pérez-Ortega, S., Ascaso, C., Haghighat, Z., Talebian, M. H., et al. (2017). Lichen colonization and associated deterioration processes in Pasargadae, UNESCO world heritage site, Iran. *Int. Biodeterior. Biodegrad.* 117, 171–182. doi:10.1016/j.ibiod.2016.12.012

Stahlschmidt, M. C., de Tapia, E. M., and del Carmen Gutiérrez-Castorena, M. (2019). A geoarchaeological investigation of the street of the Dead at the tlajinga district, teotihuacan, Mexico. *Anc. Mesoam.* 30 (1), 129–145. doi:10.1017/s0956536118000238

Steinberger, Y., Zelles, L., Bai, Q. Y., Von Lützow, M., and Munch, J. C. (1999). Phospholipid fatty acid profiles as indicators for the microbial community structure in soils along a climatic transect in the Judean Desert. *Biol. Fertil. Soils* 28, 292–300. doi:10.1007/s003740050496

Steven, B., Phillips, M. L., Belnap, J., Gallegos-Graves, L. V., Kuske, C. R., and Reed, S. C. (2021). Resistance, resilience, and recovery of dryland soil bacterial communities across multiple disturbances. *Front. Microbiol.* 12, 648455. doi:10.3389/fmicb.2021.648455

Stoops, G. (2021). *Guidelines for analysis and description of soil and regolith thin sections*. John Wiley and Sons.

Stoops, G., Marcelino, V., and Mees, F. (2010). "Micromorphological features and their relation to processes and classification: general guidelines and keys," in *Interpretation of micromorphological features of soils and regoliths* (Elsevier), 15–35.

Studlar, S. M. (1980). *Trampling effects on bryophytes: Trail surveys and experiments*. Bryologist, 301–313.

Sutherland, R., Bussen, J., Plondke, D., Evans, B., and Ziegler, a. (2001). Hydrophysical degradation associated with hiking-trail use: A case study of hawai'iloa ridge trail, O'ahu, hawai'i. *Land Degrad. Dev.* 12, 71–86. doi:10.1002/ldr.425

Tejedo, P., Benayas, J., Cajiao, D., Albertos, B., Lara, F., Pertierra, L. R., et al. (2016). Assessing environmental conditions of antarctic footpaths to support management decisions. *J. Environ. Manag.* 177, 320–330. doi:10.1016/j.jenvman.2016.04.032

Tomczyk, A. M., and Ewertowski, M. W. (2023). *Landscape degradation and development as a result of touristic activity in the fragile, high-mountain environment of Vinicunca (Rainbow Mountain), Andes, Peru*. Land Degradation and Development.

Tomczyk, A. M., Ewertowski, M. W., Creany, N., Ancin-Murguzur, F. J., Monz, C., et al. (2023). The application of unmanned aerial vehicle (UAV) surveys and GIS to the analysis and monitoring of recreational trail conditions. *Int. J. Appl. Earth Obs. Geoinf.* 123, 103474.

Tsokas, G. N., Tsourlos, P. I., Stampolidis, a., Katsonopoulou, D., and Soter, S. (2009). Tracing a major roman road in the area of ancient helike by resistivity tomography. *Archaeol. Prospect.* 16, 251–266. doi:10.1002/arp.355

Verrecchia, E. P., Ribier, J., Patillon, M., and Rolko, K. E. (1991). Stromatolitic origin for desert laminar limecrusts. *Naturwissenschaften* 78 (11), 505–507.

Verrecchia, E. P., and Trombino, L. (2021). *A visual atlas for soil micromorphologists*. Springer Nature.

Wang, Z., Erb, a. M., Schaaf, C. B., Sun, Q., Liu, Y., Yang, Y., et al. (2016). Early spring post-fire snow albedo dynamics in high latitude boreal forests using landsat-8 oli data. *Remote Sens. Environ.* 185, 71–83. doi:10.1016/j.rse.2016.02.059

Watchman, A. L., and Twidale, C. R. (2002). Relative and 'absolute'dating of land surfaces. *Earth-Science Rev.* 58 (1-2), 1–49. doi:10.1016/s0012-8252(01)00080-0

Wells, E. C. (2010). Sampling design and inferential bias in archaeological soil chemistry. *J. Archaeol. Method Theory* 17, 209–230. doi:10.1007/s10816-010-9087-7

Wikiloc (2022). Lower nahal Zeelim. Wikiblock. [online]. Available at: https://de.wikiloc.com/routen-wandern/lower-nahal-zeelim-21014675 (Accessed February 03, 2022).

Wilkinson, T. J., French, C., Ur, J. A., and Semple, M. (2010). The geoarchaeology of route systems in northern Syria. *Geoarchaeology* 25, 745–771. doi:10.1002/gea.20331

Wilkinson, T. J., Rayne, L., and Jotheri, J. (2015). Hydraulic landscapes in mesopotamia: the role of human niche construction. *Water Hist.* 7, 397–418. doi:10.1007/s12685-015-0127-9

Winterhalder, B. (1981). *Foraging strategies in the boreal forest: An analysis of Cree hunting and gathering*.

Yadin, Y. (1966). *Masada: Herod's fortress and the zealots' last stand*.

Yair, A. (1990). The role of topography and surface cover upon soil formation along hillslopes in arid climates. *Geomorphology* 3 (3-4), 287–299. doi:10.1016/0169-555x(90)90008-e

Yaşar Korkanç, S. (2014). Impacts of recreational human trampling on selected soil and vegetation properties of aladag natural park, Turkey. *Catena* 113, 219–225. doi:10.1016/j.catena.2013.08.001

Yechieli, Y., Magaritz, M., Levy, Y., Weber, U., Kafri, U., Woelfli, W., et al. (1993). Late quaternary geological history of the Dead Sea area, Israel. *Quat. Res.* 39 (1), 59–67. doi:10.1006/qres.1993.1007

Yekutieli, Y. (2006). Is somebody watching you? Ancient surveillance systems in the southern Judean Desert. *J. Mediterr. Archaeol.* 19, 65–89. doi:10.1558/jmea.2006.19.1.65

Yekutieli, Y. (2005). Landscape of control. *Anc. Near East. Stud.* 41, 5–37. doi:10.2143/anes.41.0.562919

Yekutieli, Y. (2009). The har hemar site: A northern outpost on the desert margin? *Tel Aviv* 36, 218–240. doi:10.1179/033443509x12506723940811

Zedeño, M. N., and Stoffle, R. W. (2003). *Tracking the role of pathways in the evolution of a human landscape: The st croix riverway in ethnohistorical perspective*. Routledge: The Colonization of Unfamiliar Landscapes.

Zgłobicki, W., Poesen, J., De Geeter, S., Boardman, J., Gawrysiak, L., Golosov, V., et al. (2021). Sunken lanes-Development and functions in landscapes. *Earth-Science Rev.* 221, 103757. doi:10.1016/j.earscirev.2021.103757

Zolotokrylin, a. N., Brito-castillo, L., and Titkova, T. B. (2020). Local climatically-driven changes of albedo and surface temperatures in the sonoran desert. *J. Arid Environ.* 178, 104147. doi:10.1016/j.jaridenv.2020.104147